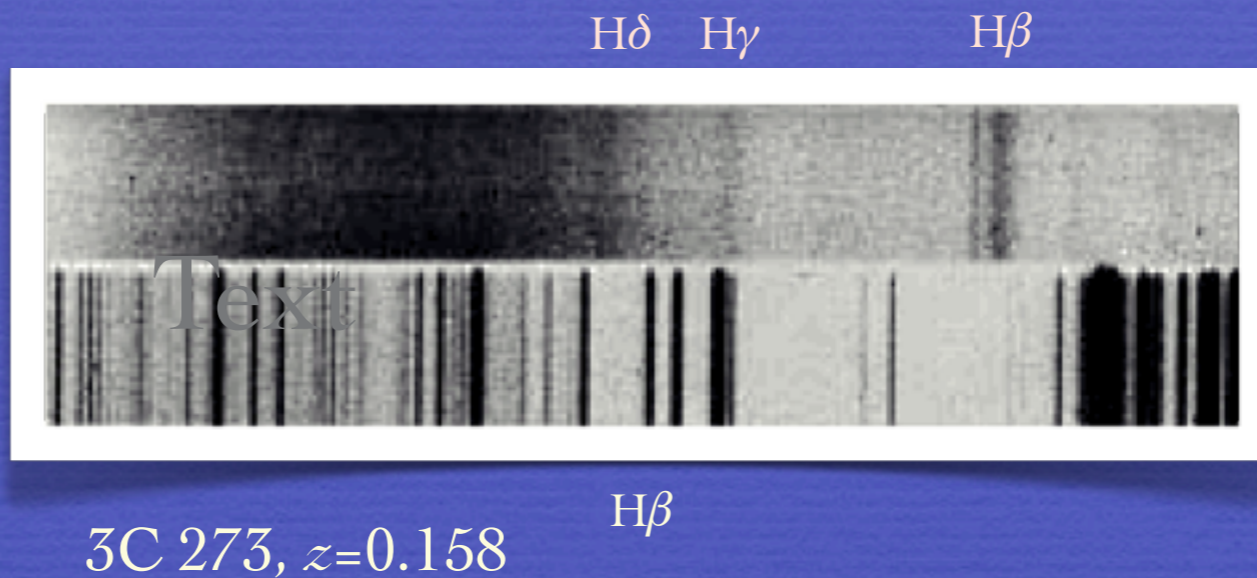
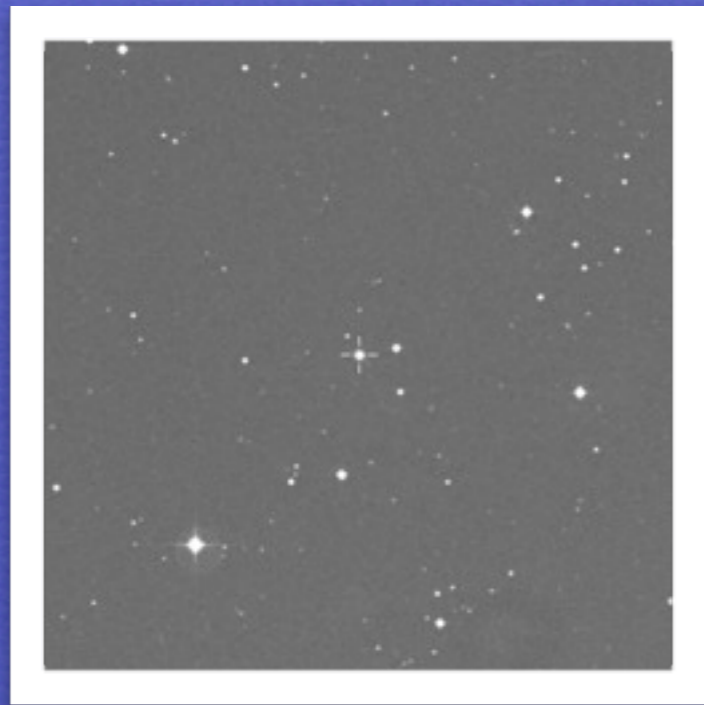


# A Photoionization Method for Black Hole Mass Estimation in Quasars<sup>☆</sup>



*Paola Marziani, INAF, Osservatorio Astronomico di Padova, Italia*

*with*

*C. Alenka Negrete (IA-UNAM), Deborah Dultzin (IA-UNAM), Jack W. Sulentic (IAA-CSIC)*

*<sup>☆</sup>Based in part on C. A. Negrete's doctoral thesis*

# Accretion onto a massive compact object

Black hole mass ( $M_{\text{BH}}$ )

Accretion rate ( $L_{\text{bol}}$ )

Physics Eddington ratio ( $L_{\text{bol}}/M_{\text{BH}}$ )

Gas chemical composition

Black hole spin (radio-loudness)

Host galaxy morphology

Aspect Viewing angle

# Virial Black Hole Mass

geometry  
dynamics

$$M_{\text{BH}} = \frac{f r (\delta v)^2}{G}$$

$r_{\text{BLR}}$

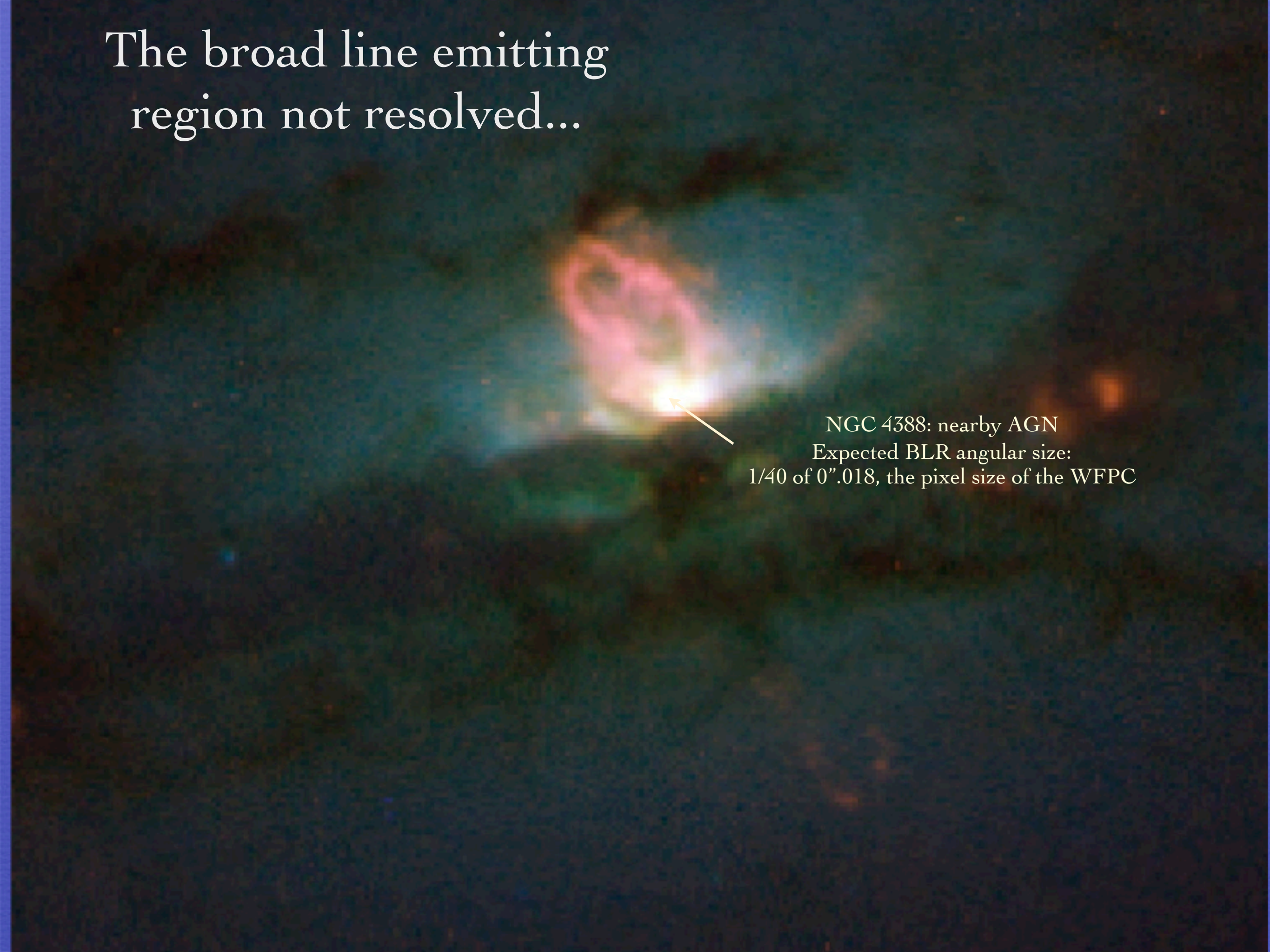
FHWM  
 $\sigma$ , FWZI

A diagram illustrating the virial black hole mass equation. The equation is  $M_{\text{BH}} = \frac{f r (\delta v)^2}{G}$ . Three callout boxes point to parts of the equation: 'geometry dynamics' points to the numerator, ' $r_{\text{BLR}}$ ' points to the variable  $r$ , and 'FHWM  $\sigma$ , FWZI' points to the velocity term  $(\delta v)^2$ .

$M_{\text{BH}}$  : if  $\delta v = \text{FWHM}$ , isotropy :  $\frac{\sqrt{3}}{2} \text{FWHM} \rightarrow f = 0.75$

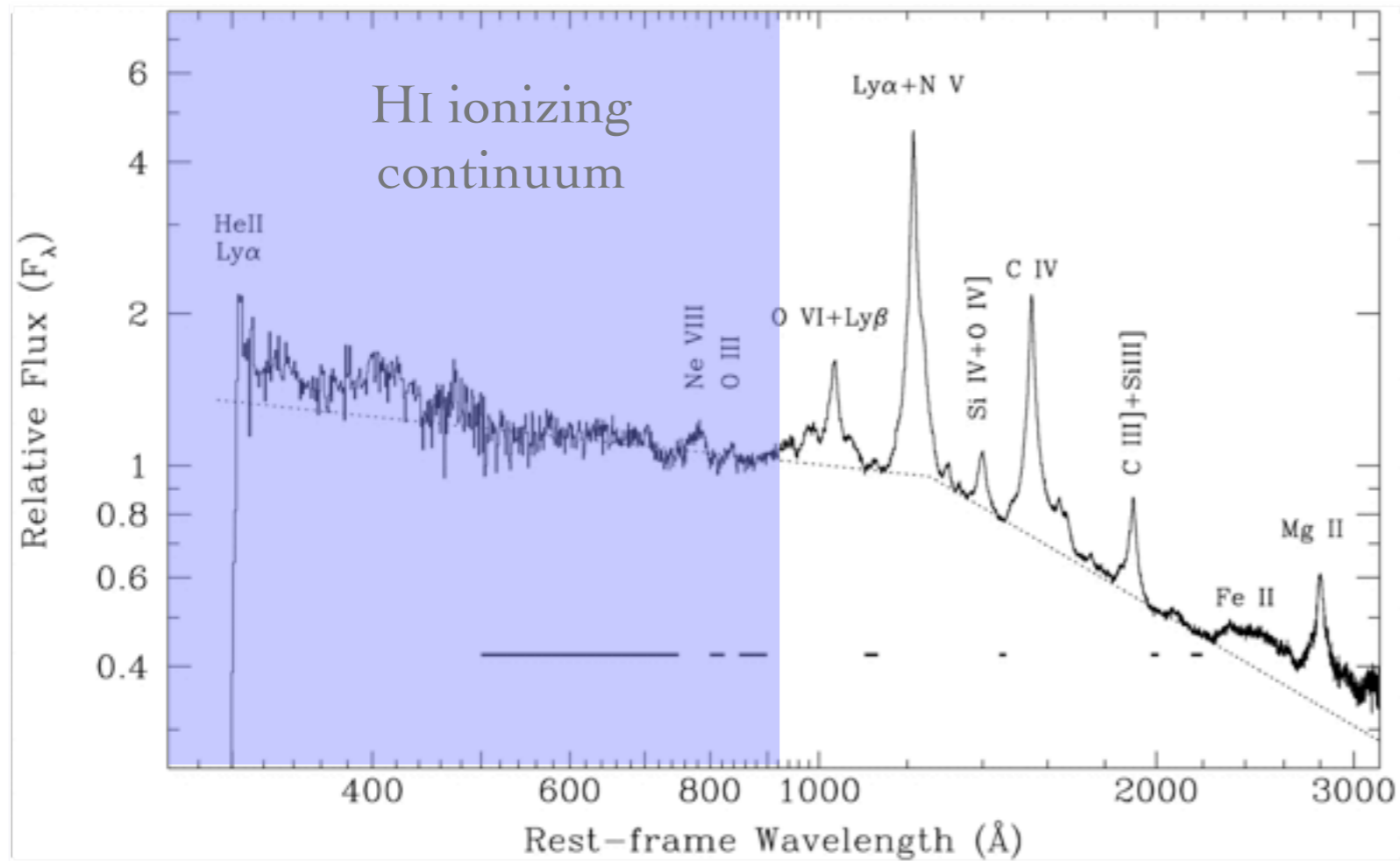
Keplerian velocity field: the BLR dynamics dominated by the gravity of a central mass;  $v \propto r^{-1/2}$

The broad line emitting  
region not resolved...

The image shows a deep-field astronomical observation of the galaxy NGC 4388. At the center, there is a bright, point-like source of light, identified as the active galactic nucleus (AGN). This central source is surrounded by a diffuse, multi-colored nebula that glows with various colors including red, orange, yellow, green, and blue. The overall appearance is that of a galaxy with a prominent central energy source. A white arrow points from the text on the right towards the central AGN.

NGC 4388: nearby AGN  
Expected BLR angular size:  
1/40 of 0".018, the pixel size of the WFPC

# The emission lines

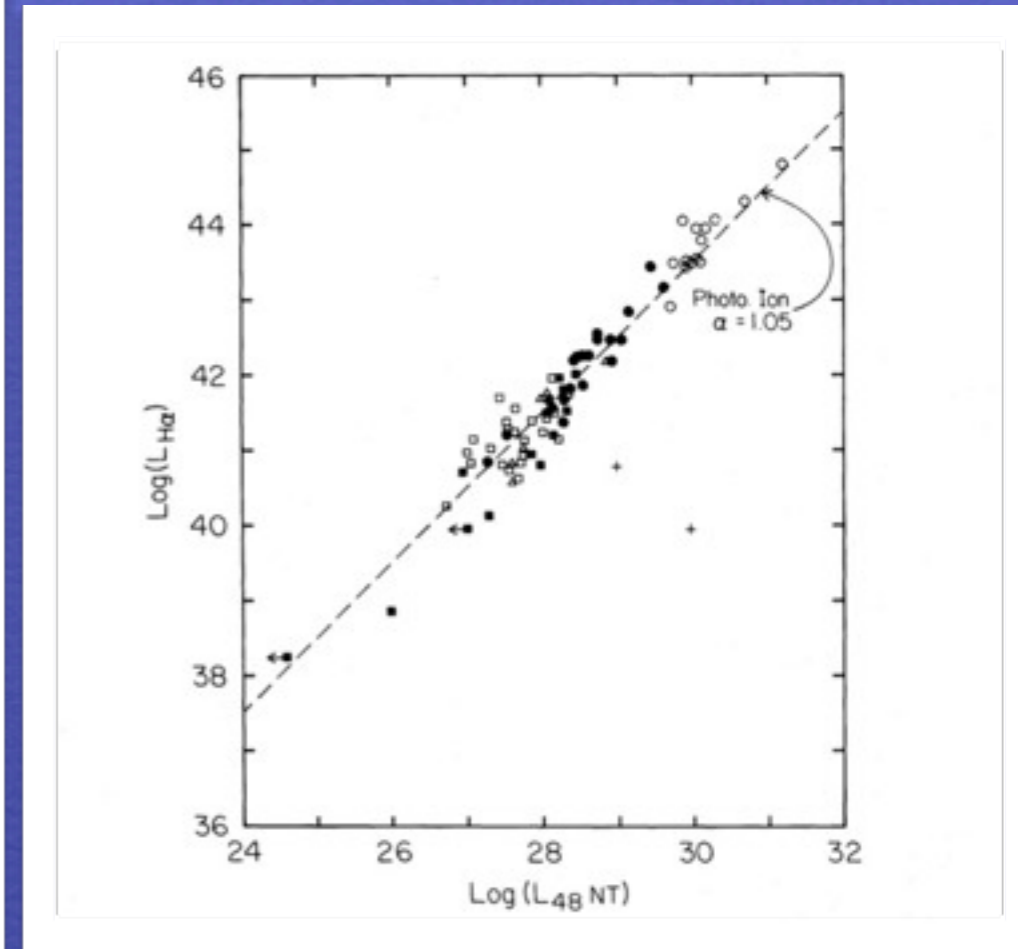


Telfer et al. 2002

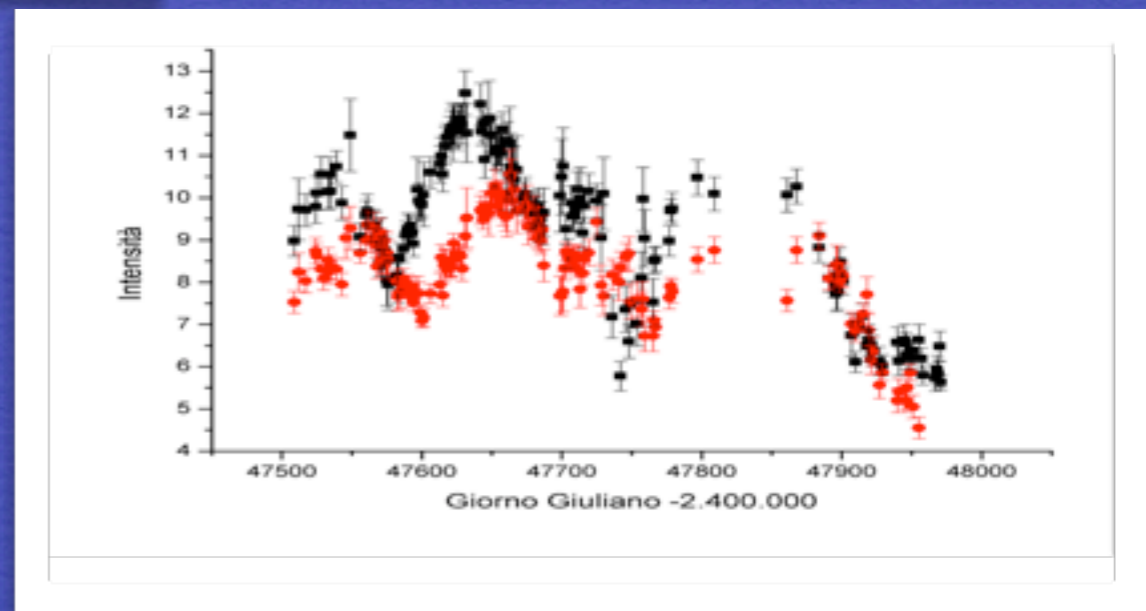
## Photoionization by FUV continuum

Line luminosity proportional to continuum luminosity;

Lines respond to continuum luminosity change



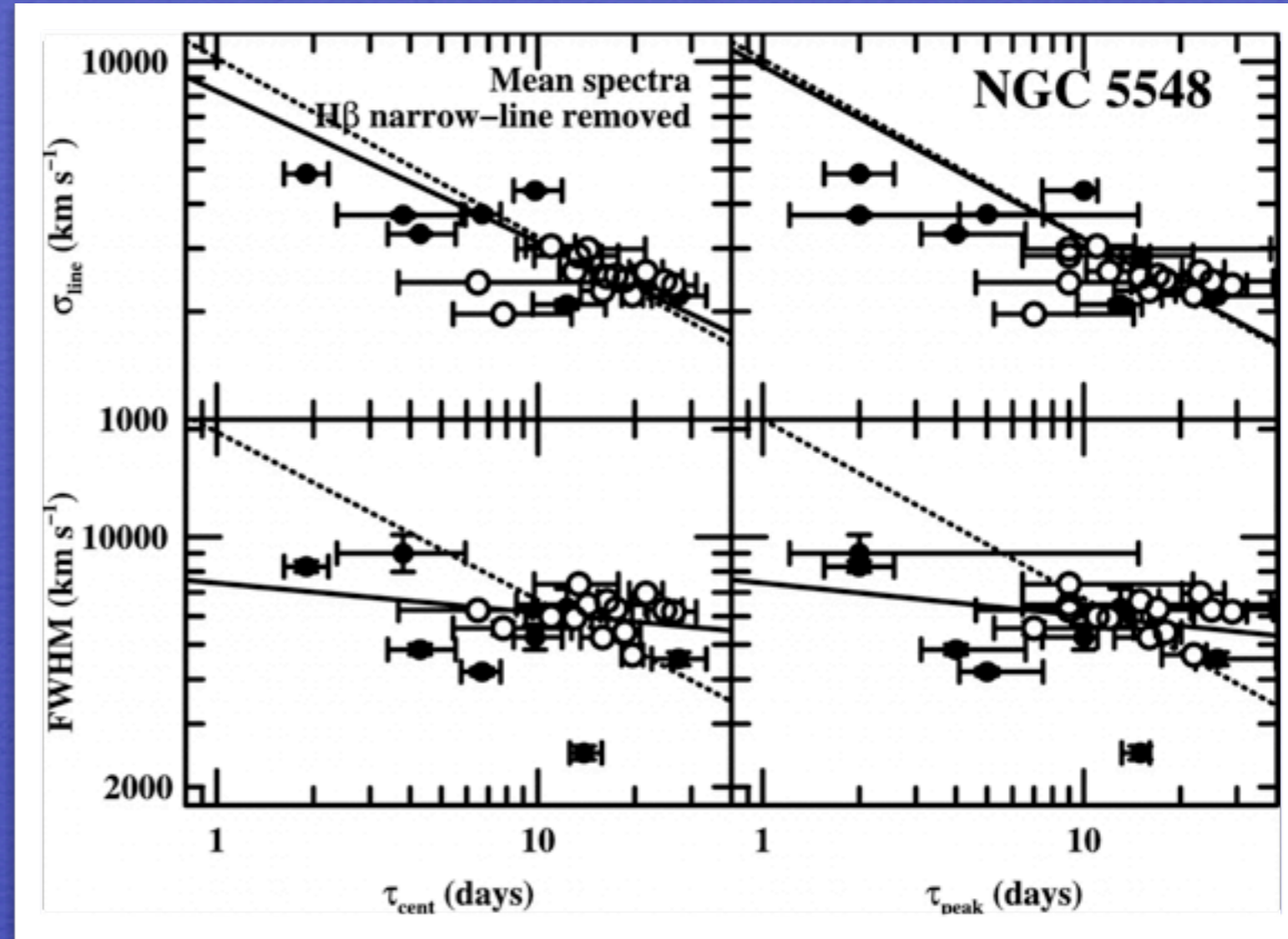
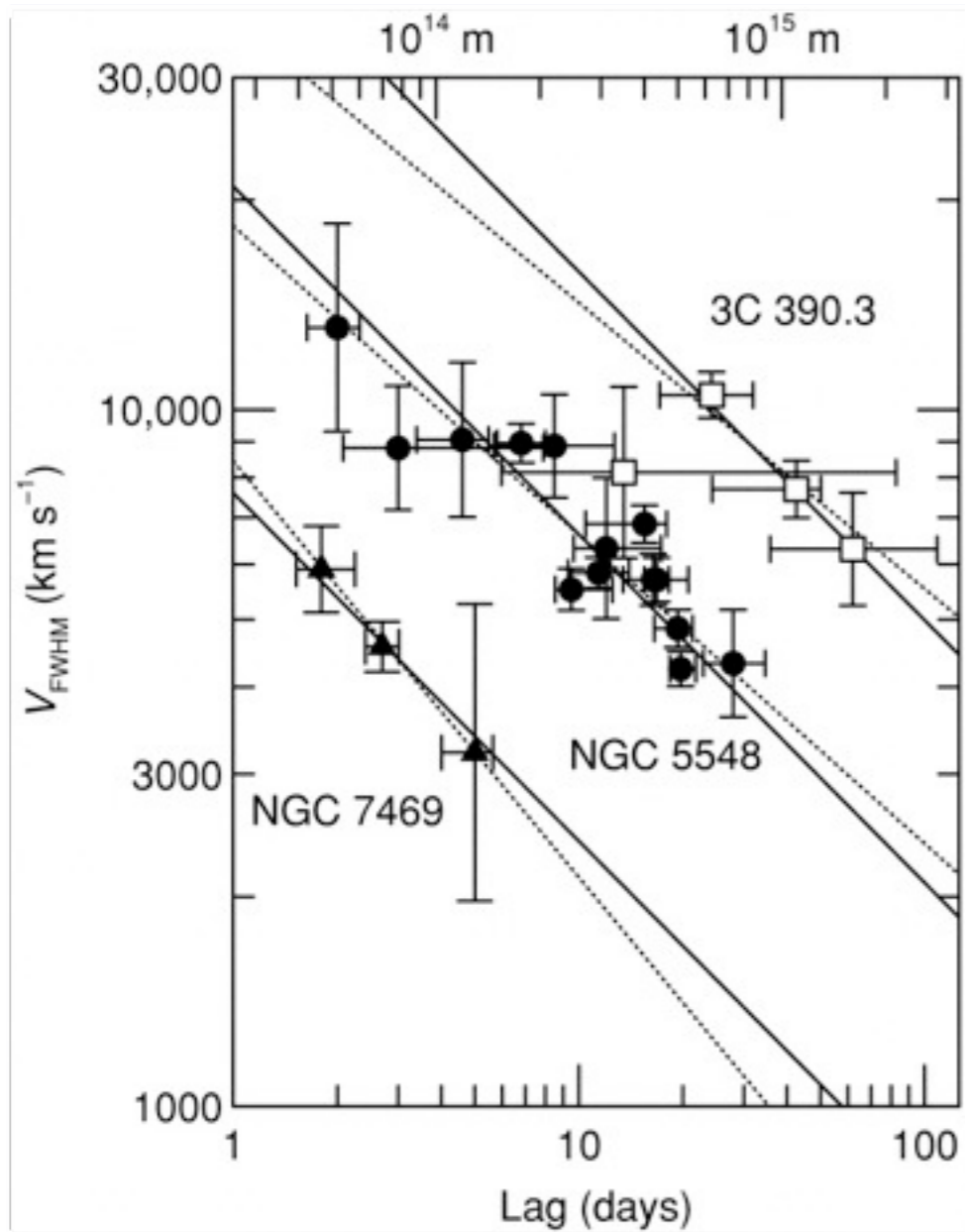
Shuder 1981



B. Peterson & the International AGN Watch

# Test of virial relationship

Peterson et al. 2004



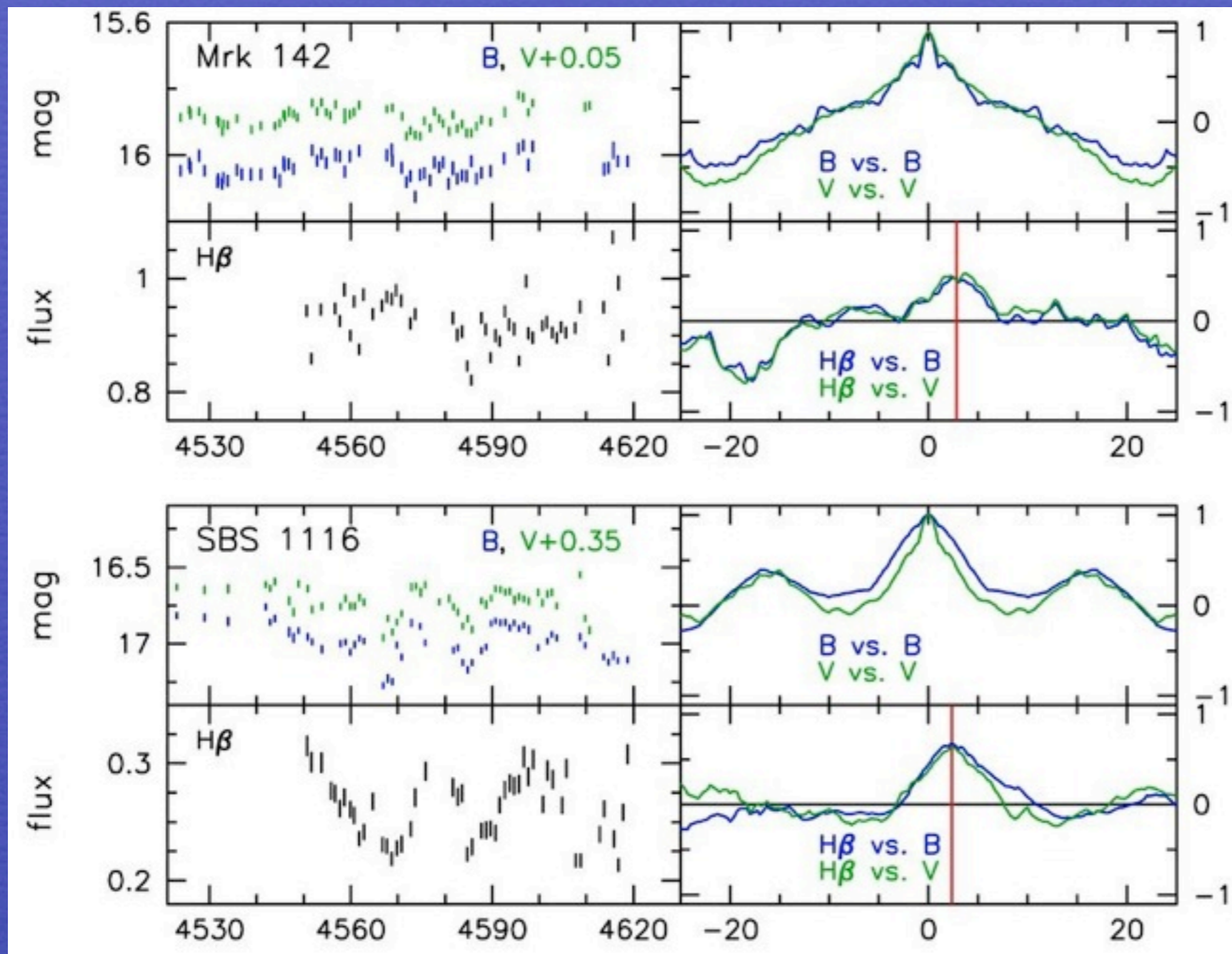
Peterson & Wandel

Best consistency with virial for rms and  $\sigma$

# Emitting region distance $r_{\text{BLR}}$ from central continuum source

Peak or (centroid) of the cross-correlation function between line and continuum

$$\text{CCF}(\tau) = \int \mathcal{L}(t)\mathcal{C}(t - \tau)dt$$



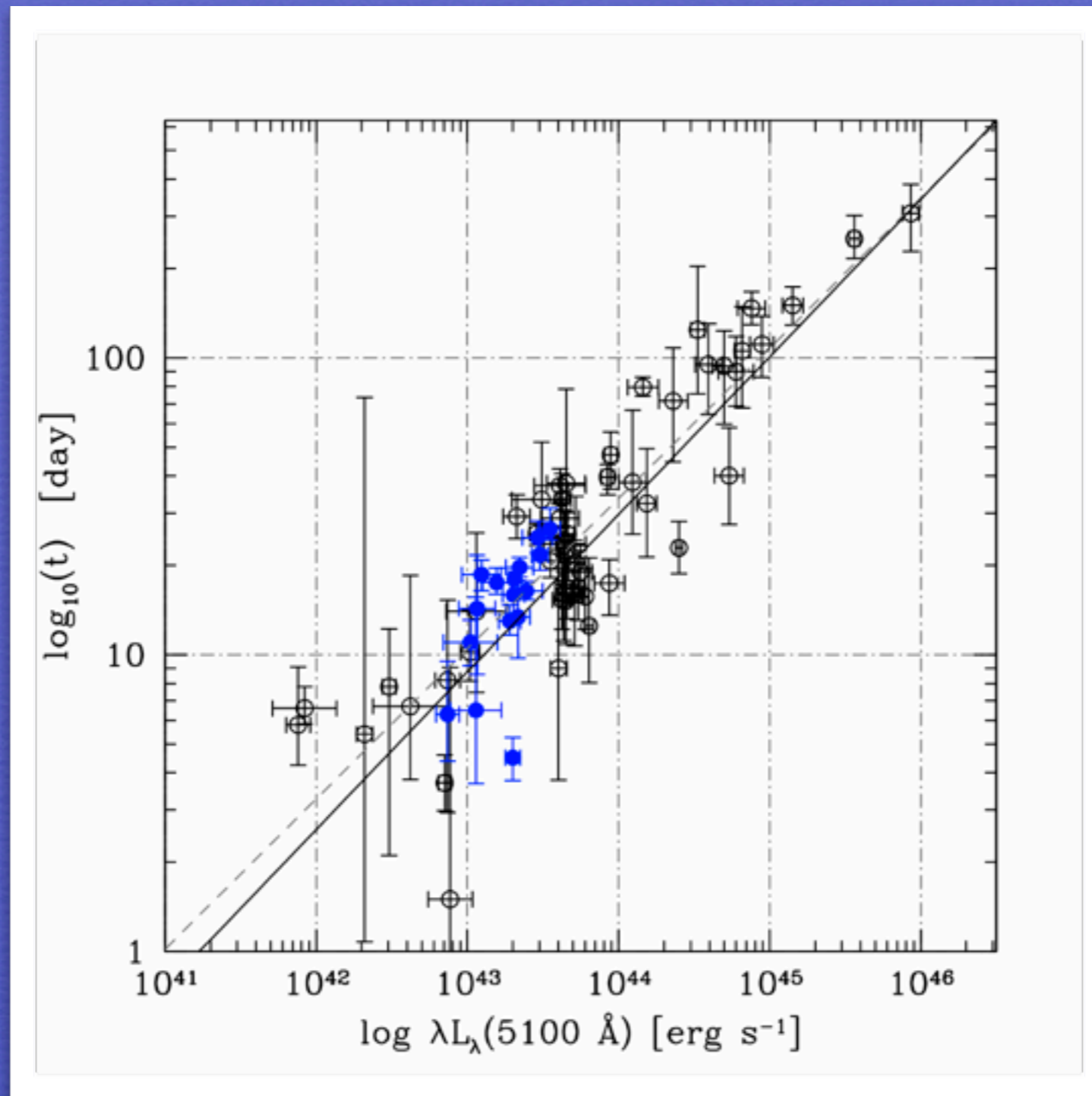
$$r_{\text{BLR}} = c\tau_{\text{H}\beta}$$

from H $\beta$   
monitoring is  
available for

~50 low- $z$   
AGN as of  
Dec. 2010

(Kaspi et al., Bentz, et al. 2009)

# $r_{\text{BLR}}$ indirect (“secondary”) determination from $\text{H}\beta$

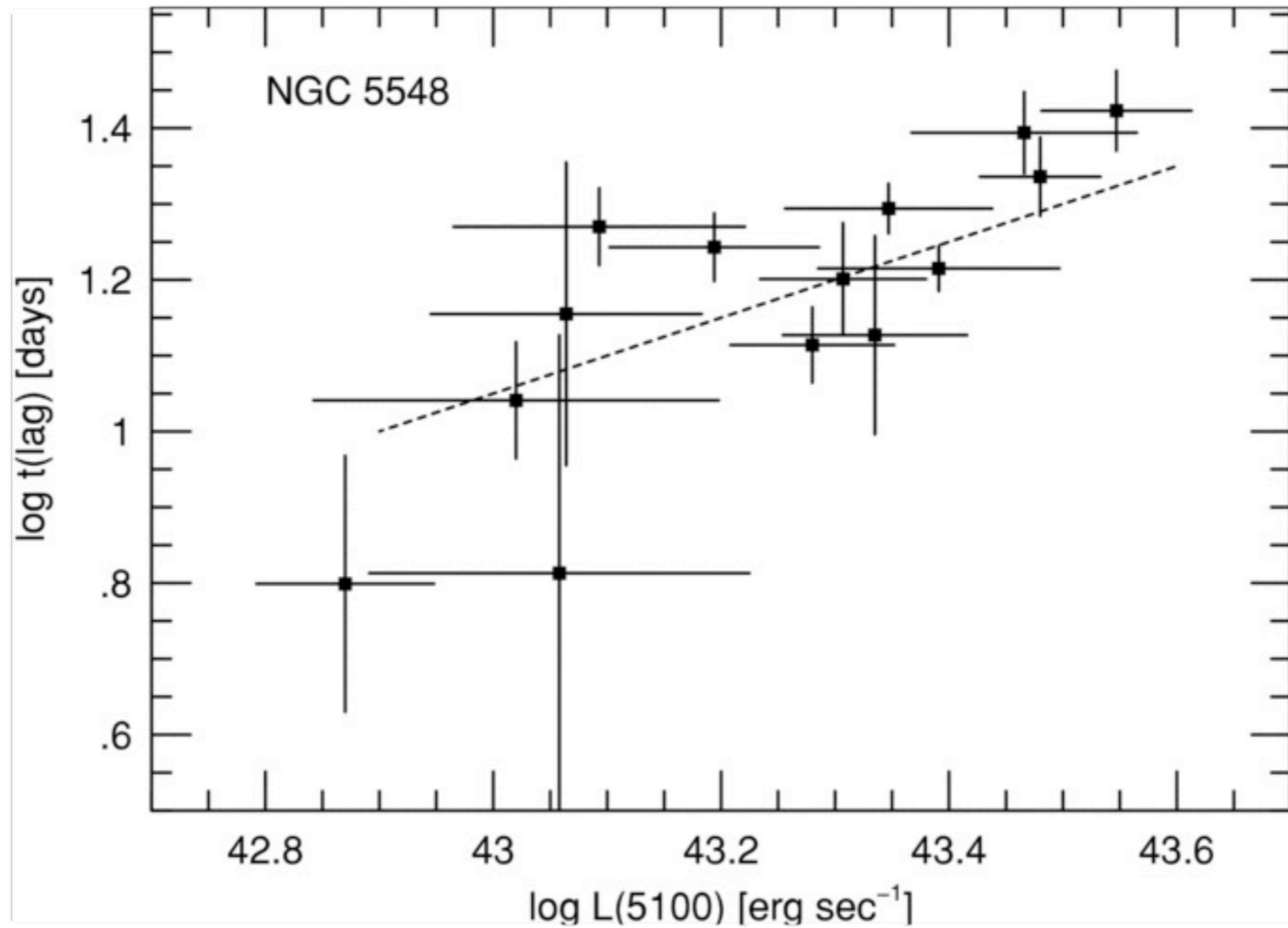


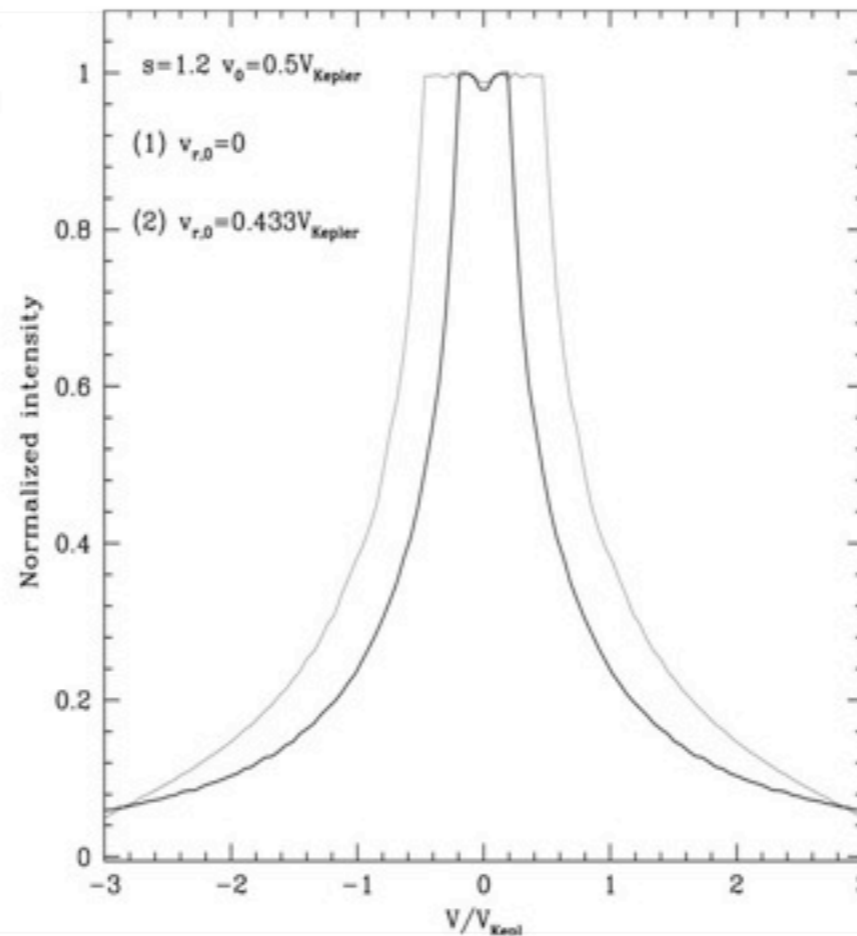
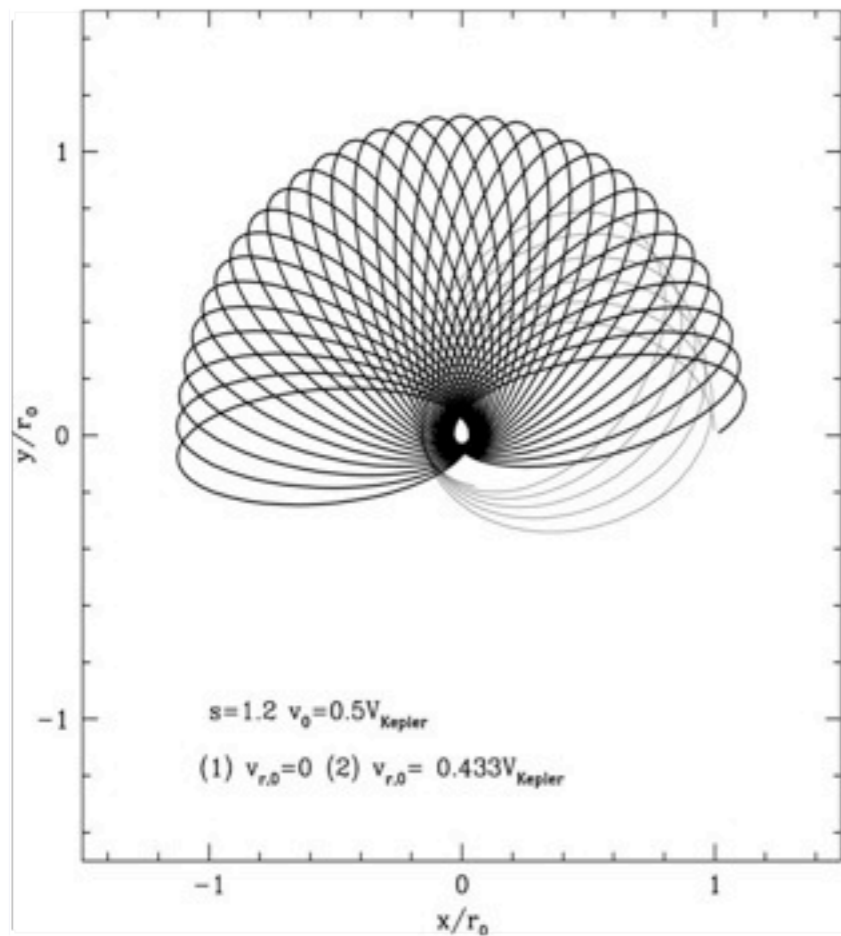
(all determinations data from  
Bentz. et al. 2009; cf.  
Kaspi et al., 2000,2005)

$r_{\text{BLR}}$  correlates with  $L^a$   
 $a \sim 0.5 - 0.7$ , with  $a \approx 0.52$  now favored



# Continuum luminosity is affecting the response time





Effect of radiation pressure on  $f$  on a system of clouds

Netzer & Marziani 2010

$$M_{\text{BH}} = f r (\delta v)^2 G^{-1}$$

**Table 1**

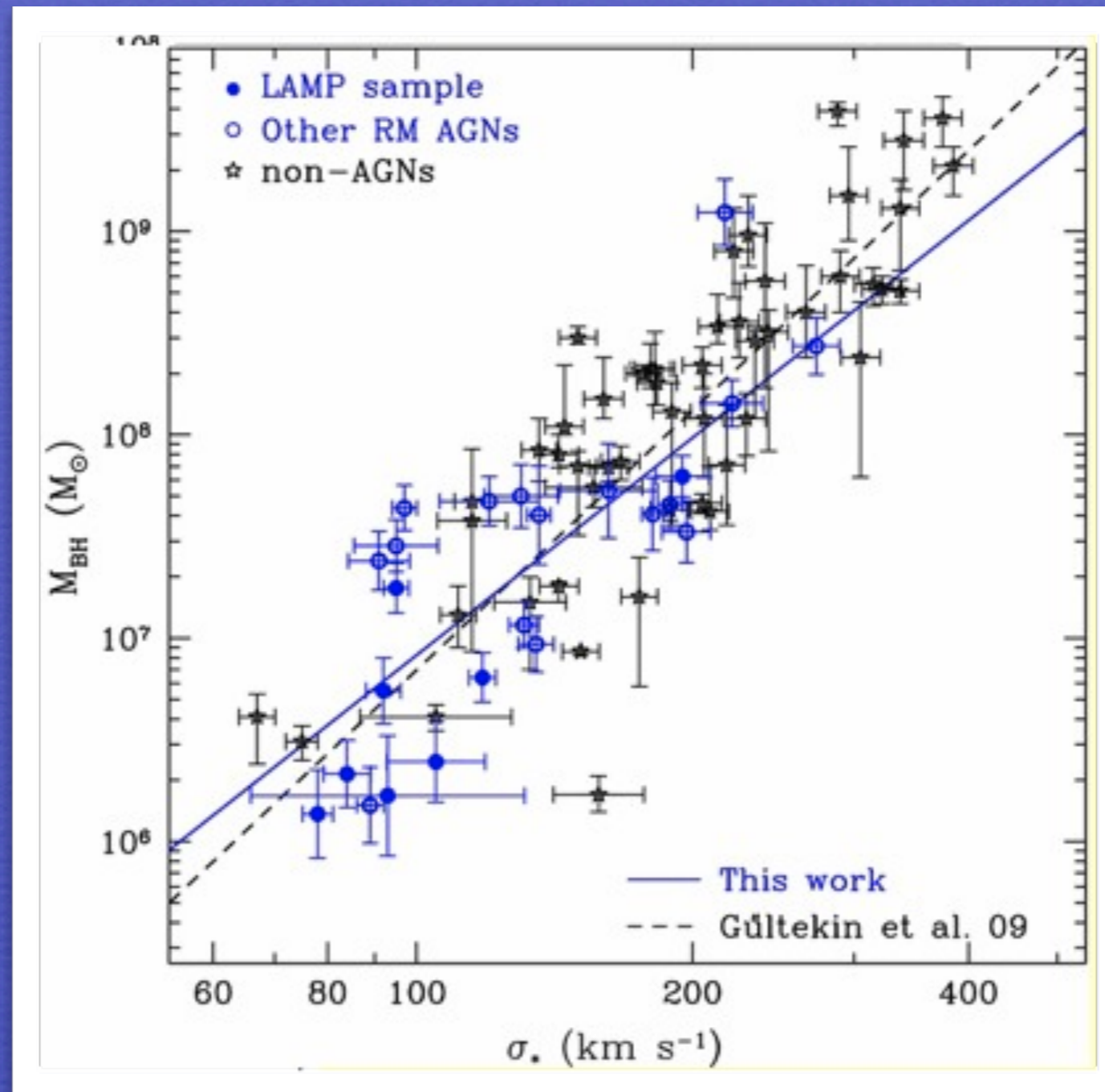
Line Widths, Mass Conversion Factor  $f$ , and Emissivity-weighted Radii for Various Models Assuming the Line Emissivity is Strictly Proportional to the Cloud Cross Section and  $\alpha(r) = 0.5$

$\Gamma$	FWHM/ $v_{\text{Kepler}}(r_0)$	$\langle r \rangle / r_0$	$f$
$s = 1.2$	$r_{23} = 10r_0$	$v_0 = 0.5$	
0.05	1.58 (0.93)	0.54	0.75 (2.18)
0.1	1.55 (0.92)	0.54	0.77 (2.21)
0.3	1.45 (0.87)	0.56	0.85 (2.37)
0.5	1.34 (0.81)	0.59	0.94 (2.56)
0.7	1.15 (0.72)	0.68	1.11 (2.78)
0.735	1.06 (0.68)	0.78	1.13 (2.76)

# $M_{\text{BH}}$ vs. bulge stellar velocity dispersion

Geometry factor  $f$  obtained scaling the  $M_{\text{BH}}$  to agree with the dynamical masses

Results have varied widely:  
 $f(\text{FWHM}) \approx 2$   
Woo et al. 2010

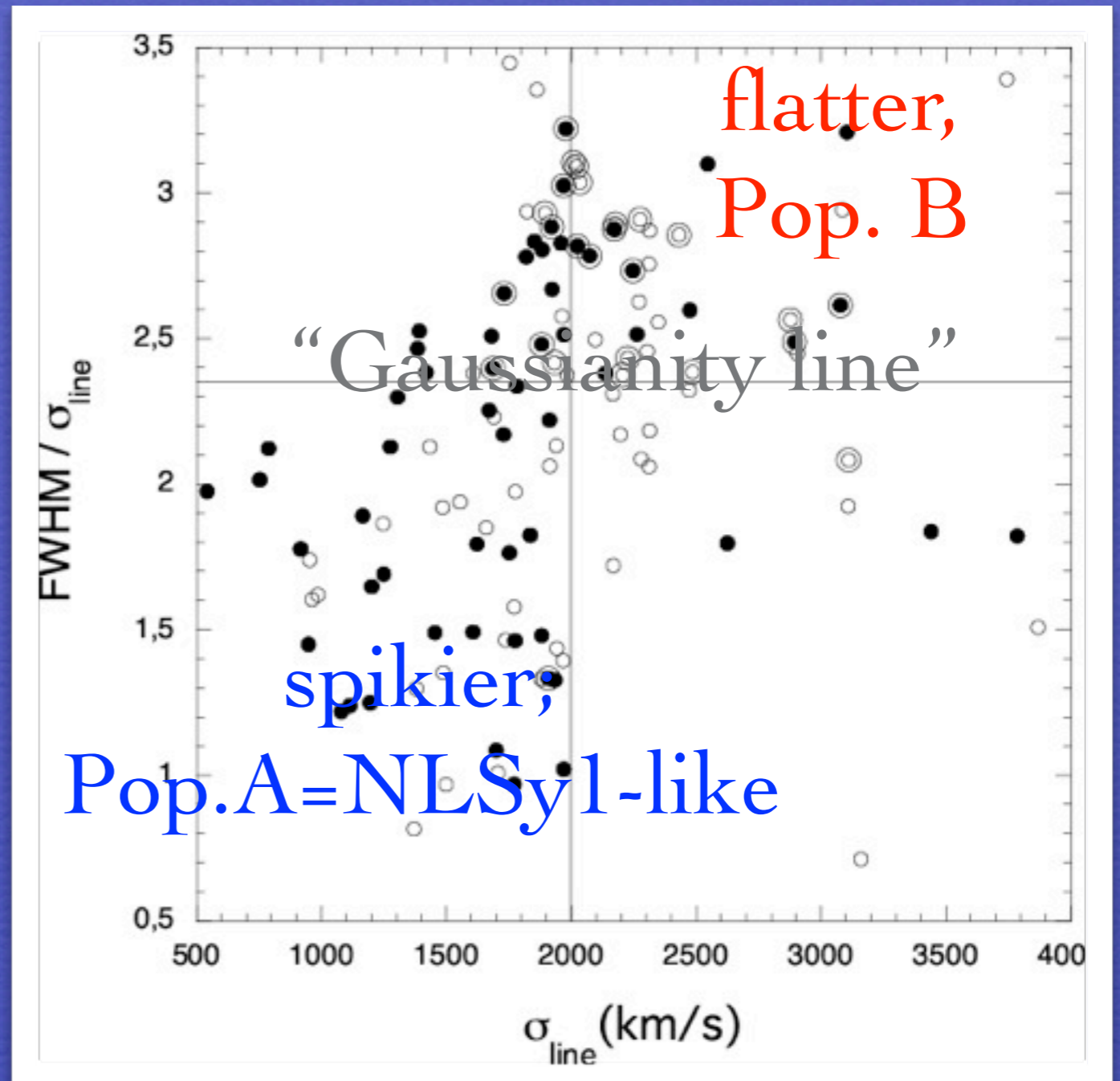


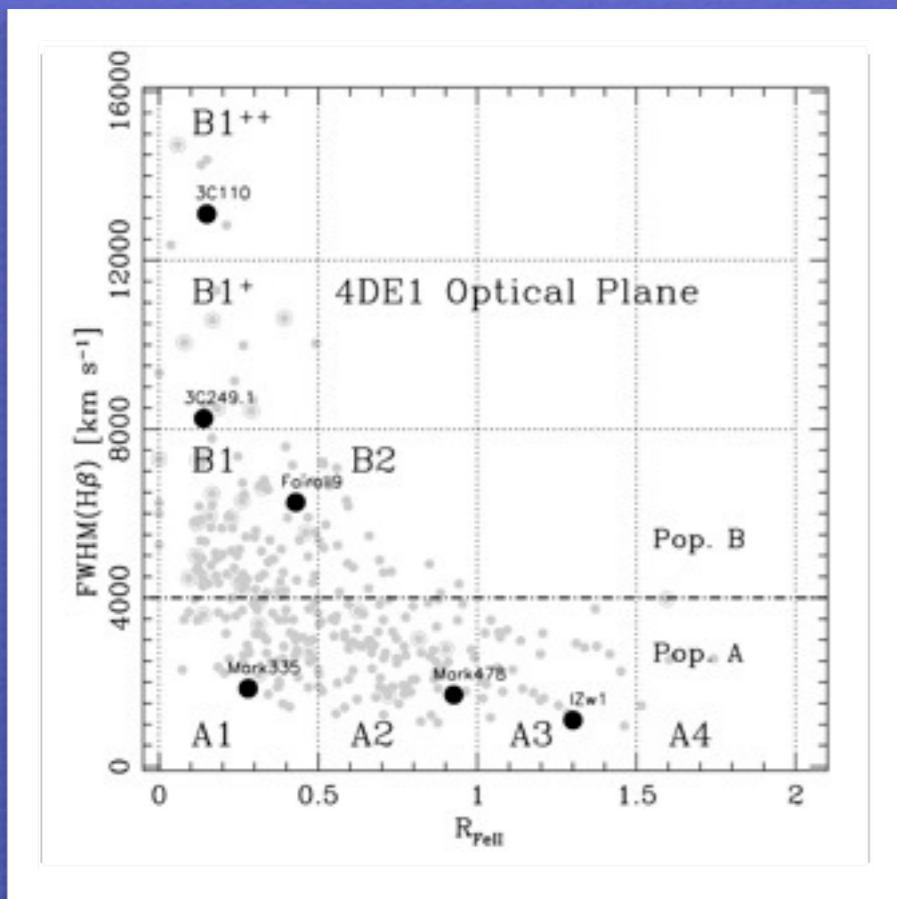
$f$  is most likely dependent on profile shape

**Table 2.** The scale factors with their uncertainties for the Onken sample and for two populations (1) separated at  $FWHM/\sigma_{line} = 2.35$  (Pop1 and Pop2) as explained in the text and (2) separated at  $FWHM = 4000 \text{ km s}^{-1}$  (PopA and PopB) according to Sulentic et al. (2000).

	$f(\sigma_{line})$	$df(\sigma_{line})$	$f(FWHM)$	$df(FWHM)$
MEAN SPECTRUM				
total	3.85	1.15	1.17	0.50
Pop1	4.20	2.09	1.81	1.38
Pop2	3.48	1.09	0.69	0.19
PopA	3.93	1.97	2.12	1.47
PopB	3.75	1.13	0.52	0.13
RMS SPECTRUM				
total	5.49	1.65	1.44	0.49
Pop1	5.36	2.71	2.21	1.22
Pop2	5.66	1.49	0.92	0.27
PopA	6.23	3.47	2.53	1.49
PopB	4.73	1.11	0.81	0.19

Collin et al. 2006

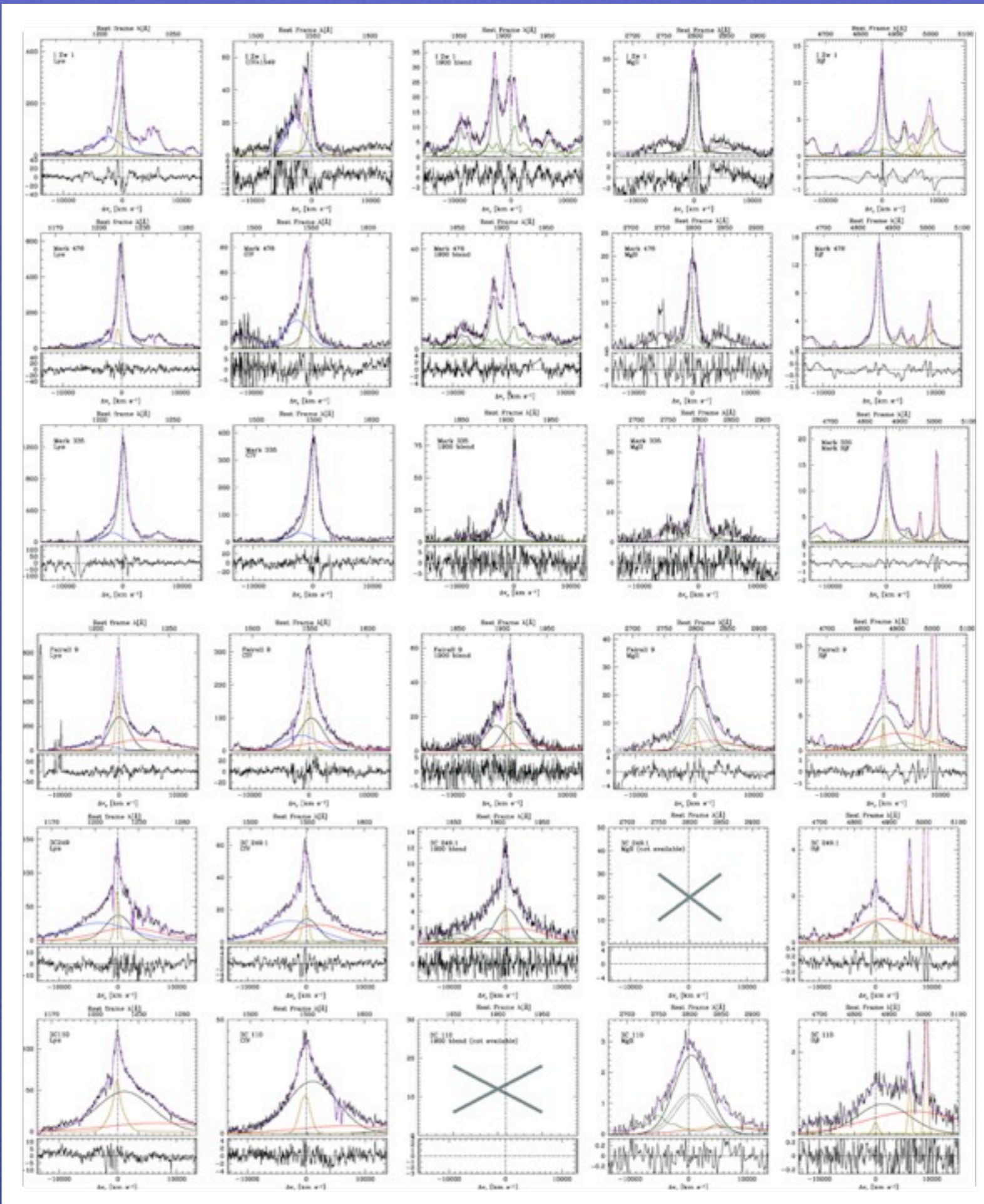


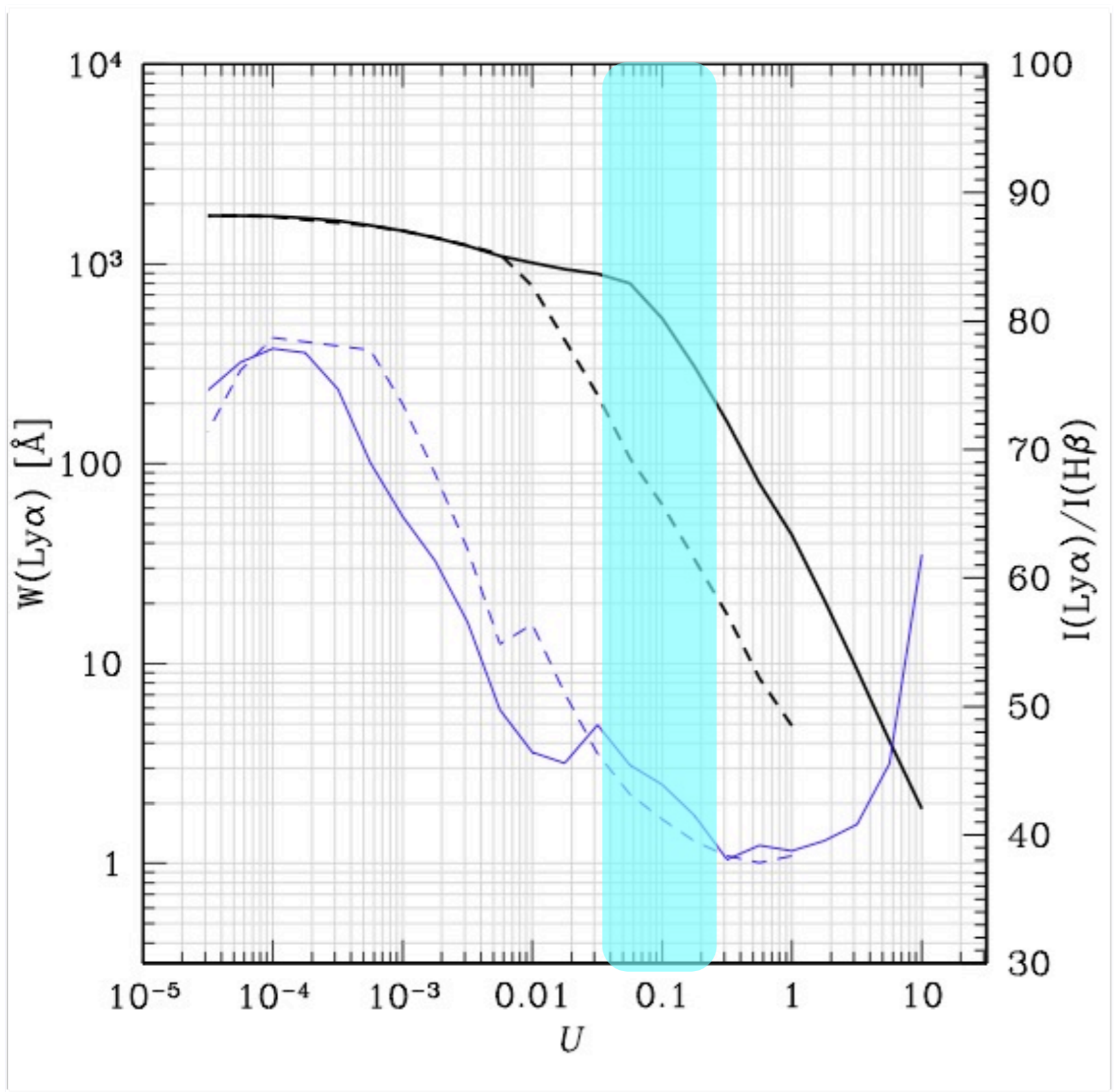


Blueshifted component: strong in  $Ly\alpha$ ,  $CIV\lambda 1549$ ,  $HeII\lambda 1640$

“Broad Component”: strong in all Low ionization lines:  $FeII$ ,  $AlIII\lambda 1860$ ,  $MgII\lambda 2800$ ,  $H\beta$

“Very Broad Component”: strong in  $Ly\alpha$ ,  $CIV\lambda 1549$ , Balmer lines of Population B sources only; absent in  $FeII$





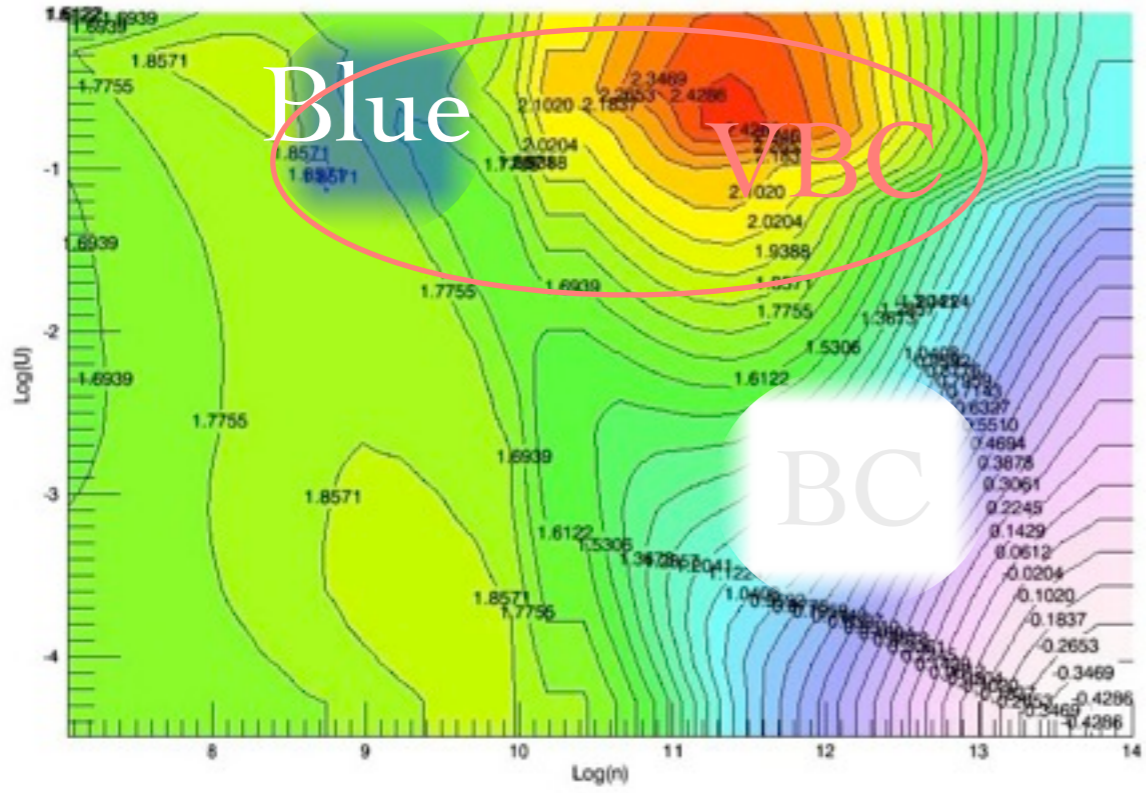
Blueshifted component:  
 large  $Ly\alpha/H\beta$

$H\beta$  detected only in median spectra or in extreme objects

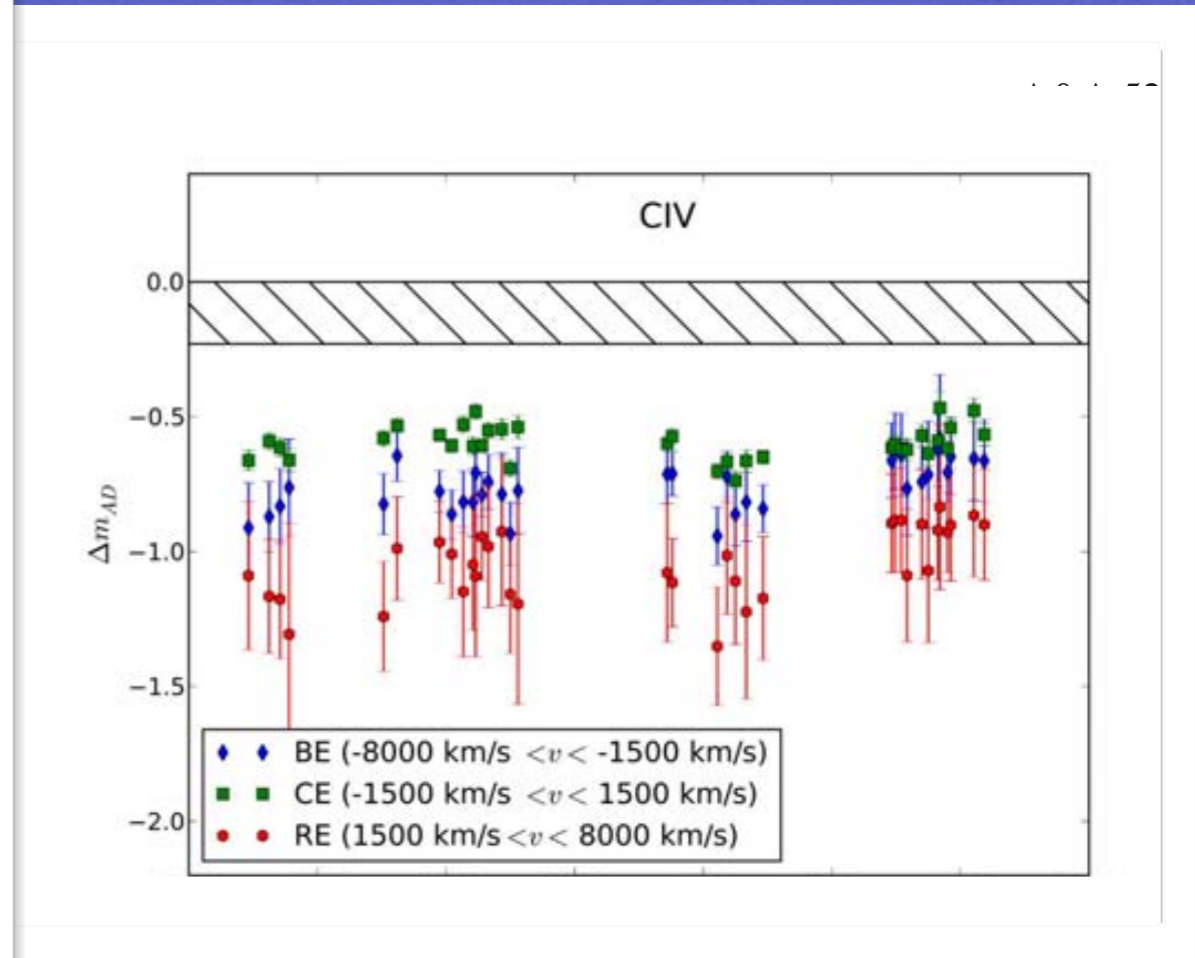
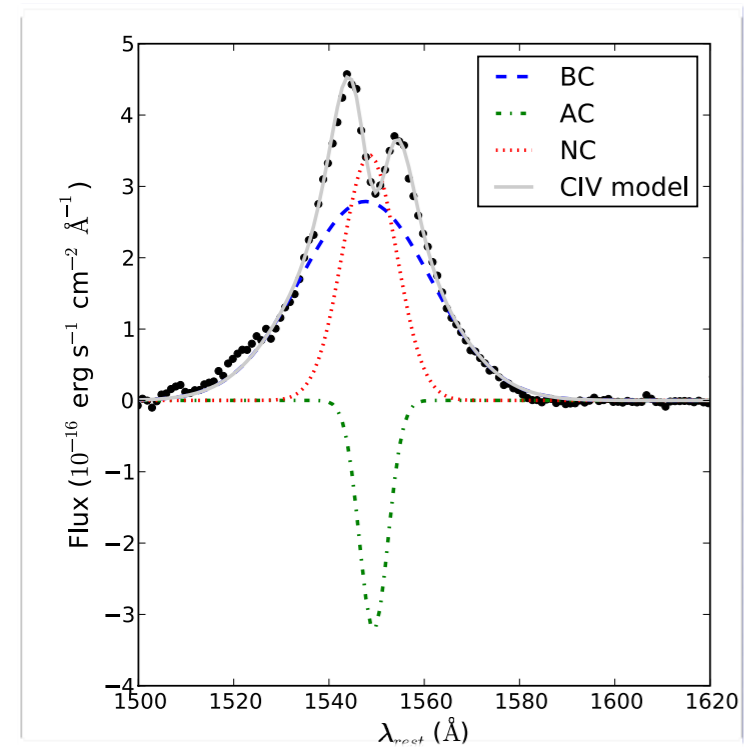
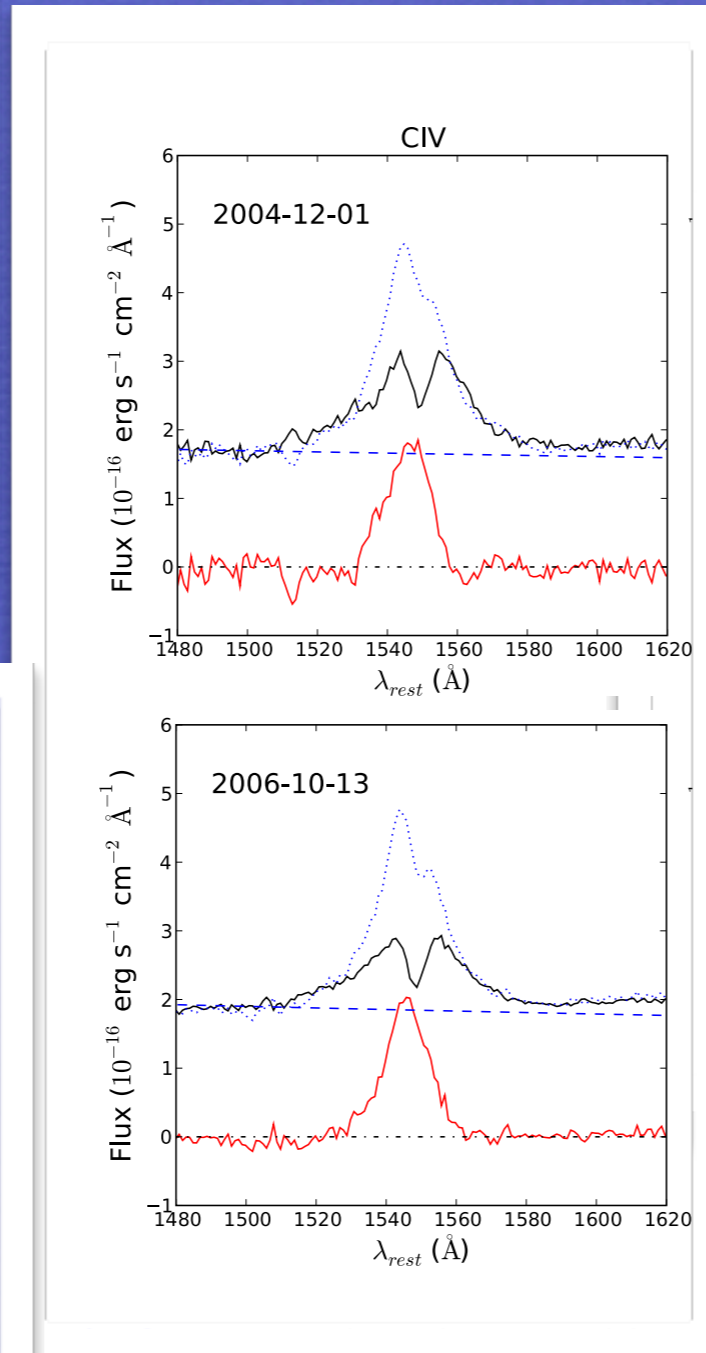
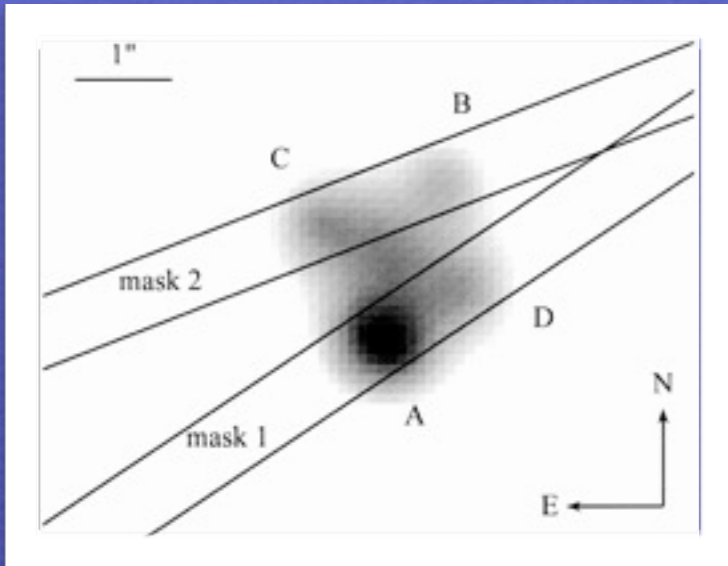
Very different from the other components for which  $Ly\alpha/H\beta \sim 5 - 10$

$$U = \frac{\text{number density of ionizing photons}}{\text{electron density}}$$

Lysalpha/ Hbeta



# A microlensing study of the Einstein cross (QSO 2237+0305): CIV results





POP A: HIL WIND (BLUESHIFTED COMPONENT)

moderate  $N_c$ , low density, high ionization

weaker in Pop. B and especially radio-loud sources

NON VIRIAL

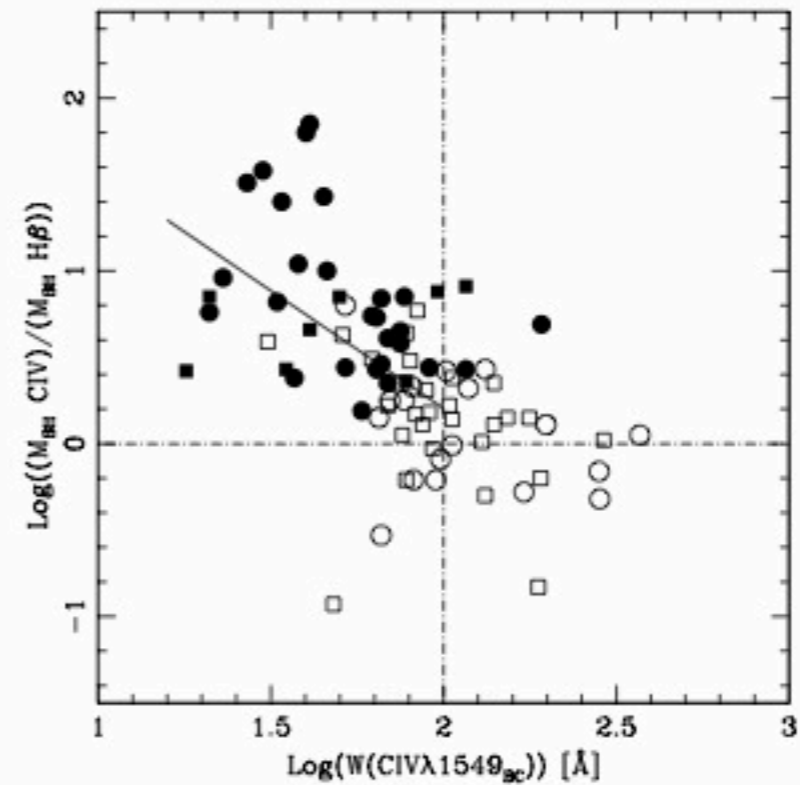
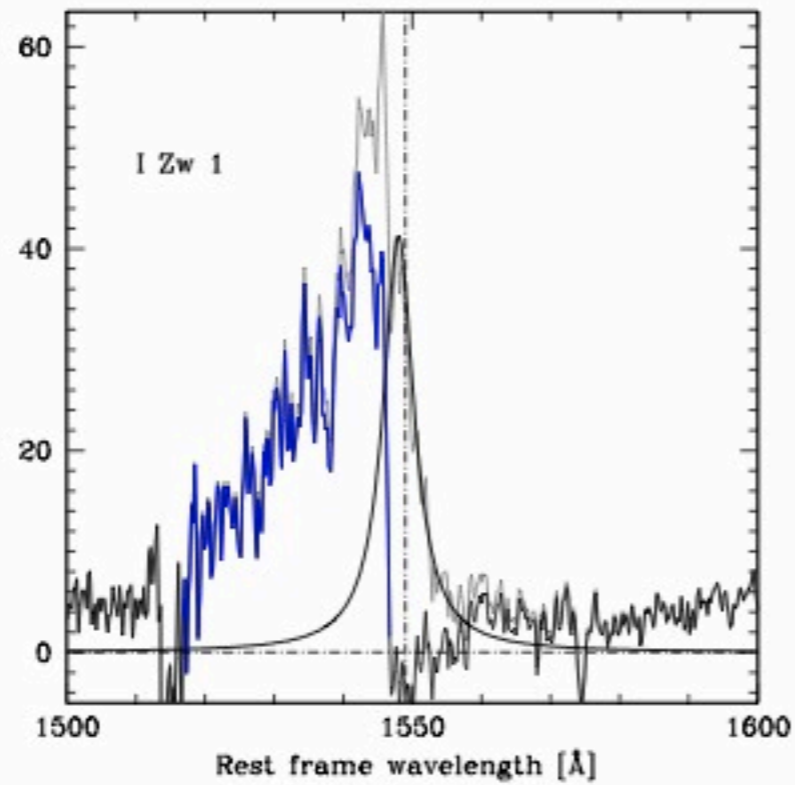
POP B: VERY BROAD COMPONENT

high ionization, large  $N_c$ , large range of density

HIL, LIL stratified emitting region from BC to VBC

NON VIRIAL

# Including non virial components:



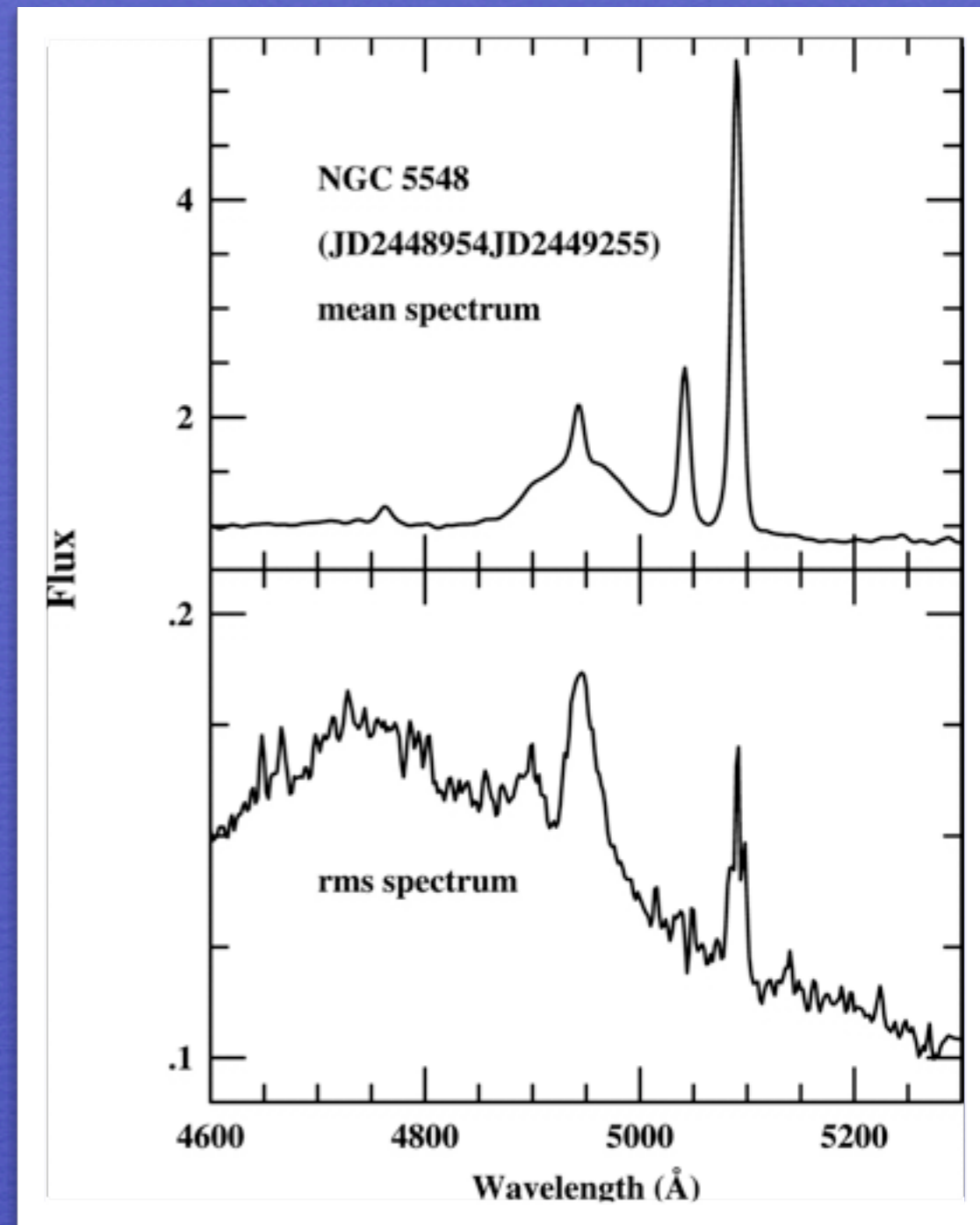
## BROAD COMPONENT

emitting all LILs, low  
ionization, high density,  
large  $N_c$

presumed VIRIAL  
component whose

width

can be used for  $M_{BH}$   
computations



Peterson et al. 2004

Single epoch approximation to the  
reverberating part of the line

# “Photoionization” mass computations

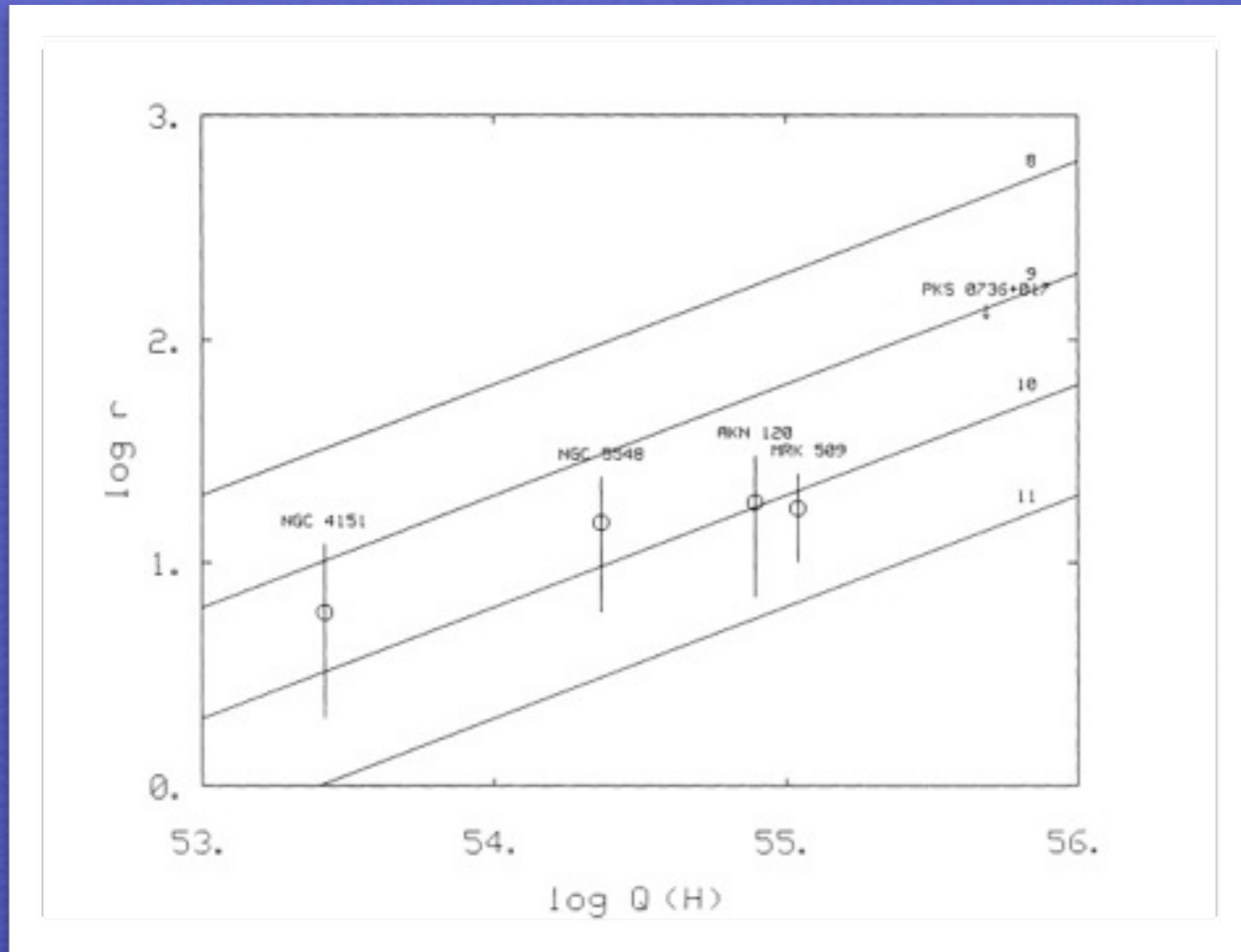
$$M_{\text{BH}} = \frac{f r_{\text{BLR}} (\text{FWHM})^2}{G}$$

$$U = \frac{\int_{\nu_0}^{+\infty} \frac{L_\nu}{h\nu} d\nu}{4\pi r_{\text{BLR}} n_e c}$$

$$r_{\text{BLR}} = \left( \frac{\int_{\nu_0}^{+\infty} \frac{L_\nu}{h\nu} d\nu}{4\pi U n_e c} \right)^{\frac{1}{2}}$$

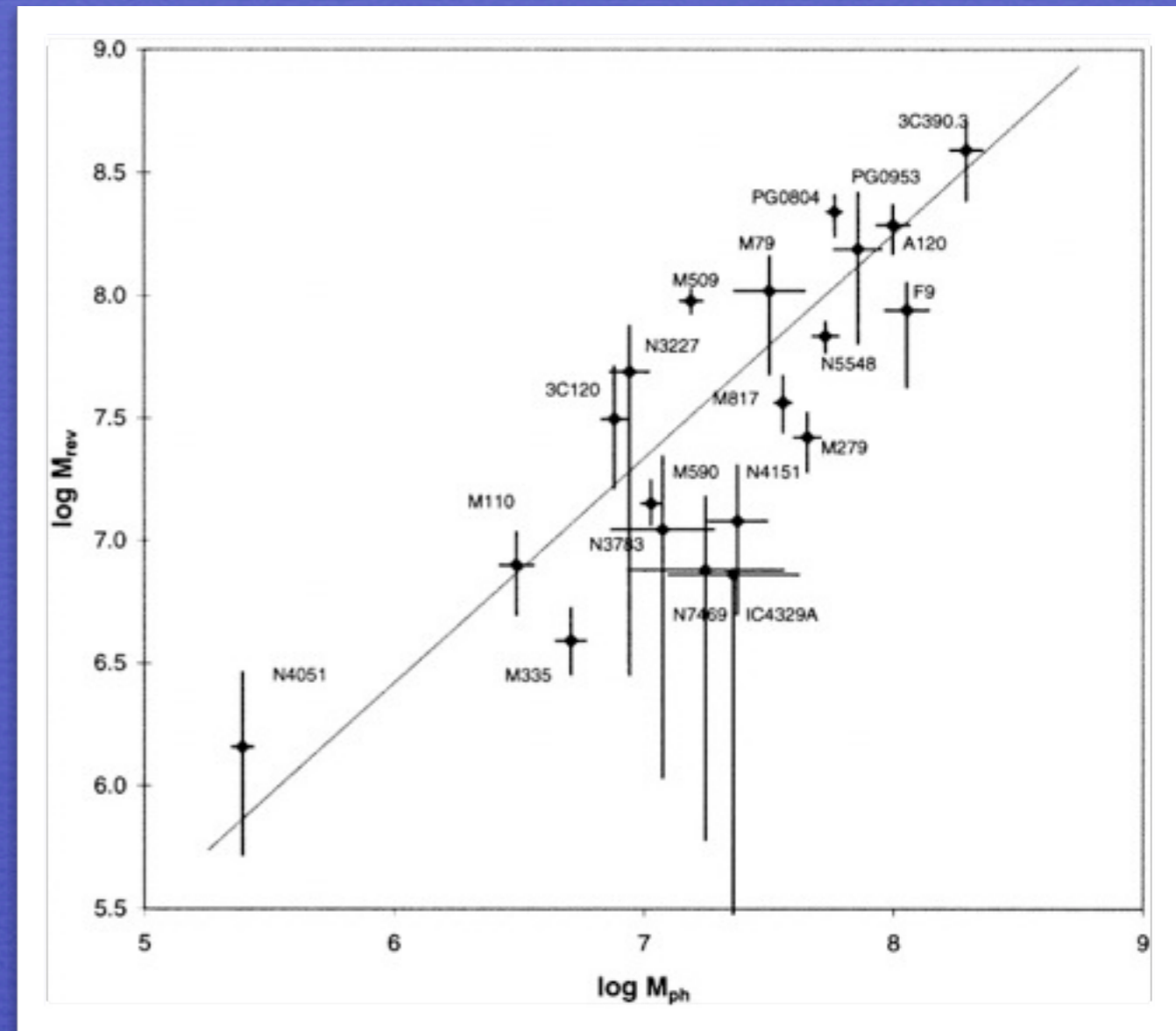
$$r_{\text{BLR}} = \underbrace{\frac{1}{(4\pi c)^{\frac{1}{2}}}}_{\text{const.}} \underbrace{(U n_e)^{-\frac{1}{2}}}_{\text{diagnostics}} \left( \underbrace{\int_{\nu_0}^{+\infty} \frac{L_\nu}{h\nu} d\nu}_{\# \text{ ionizing photons}} \right)^{\frac{1}{2}}$$

# Reverberation of H $\beta$



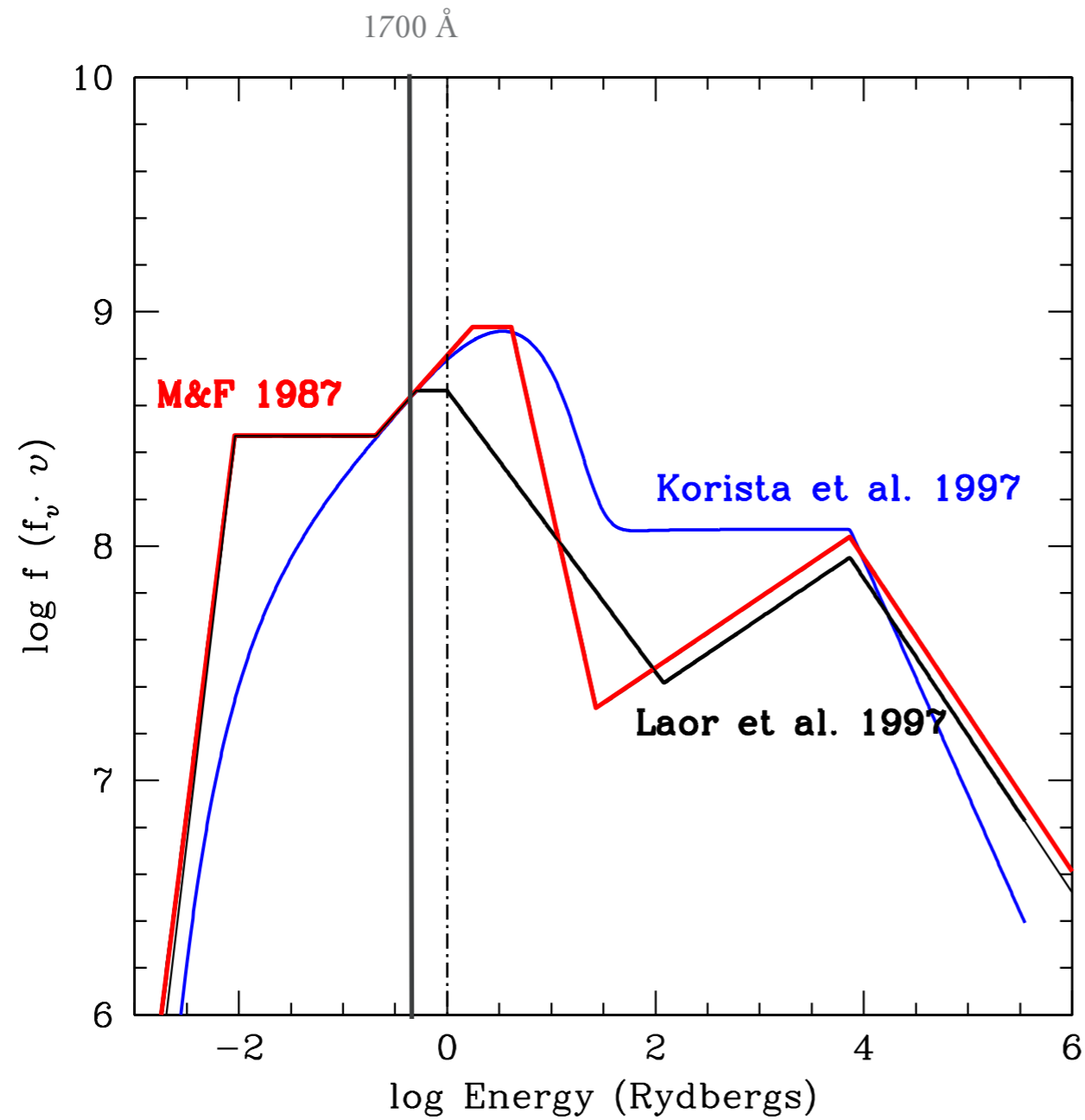
Padovani 1988

$$(U_n) \approx 10^{9.8} \text{ cm}^{-3}$$



Wandel et al. 1999

# Number of ionizing photons



Same  $f_\lambda$  at  $1700 \text{ \AA}$   $\Rightarrow$   
 $Q(\text{H})(\text{M\&F}) \approx 2Q(\text{H})(\text{L97})$

# Diagnostics from the rest-frame UV spectrum

TABLE 1  
LINES IN THE 1350-2000 Å SPECTRAL RANGE

Ion	$\lambda$ [Å]	$X$ [eV]	$E_l - E_u$ [eV]	Transition	$A_{ki}$ [s <sup>-1</sup> ]	$n_c$ [cm <sup>-3</sup> ]	Note
Si IV	1393.755	45.20	0.000 - 8.896	$2P_{3/2}^o \rightarrow 2S_{1/2}$	$8.80 \cdot 10^8$	...	1
Si IV	1402.770	45.20	0.000 - 8.839	$2P_{1/2}^o \rightarrow 2S_{1/2}$	$8.63 \cdot 10^8$	...	1
C IV	1548.202	47.89	0.000 - 8.008	$2P_{3/2}^o \rightarrow 2S_{1/2}$	$2.65 \cdot 10^8$	...	1
C IV	1550.774	47.89	0.000 - 7.995	$2P_{1/2}^o \rightarrow 2S_{1/2}$	$2.64 \cdot 10^8$	...	1
Si II	1808.00	8.15	0.000 - 6.857	$2D_{3/2}^o \rightarrow 2P_{1/2}$	$2.54 \cdot 10^6$	...	1
Si II	1816.92	8.15	0.036 - 6.859	$2D_{5/2}^o \rightarrow 2P_{3/2}$	$2.65 \cdot 10^6$	...	1
Al III	1854.716	18.83	0.000 - 6.685	$2P_{3/2}^o \rightarrow 2S_{1/2}$	$5.40 \cdot 10^8$	...	1
Al III	1862.790	18.83	0.000 - 6.656	$2P_{1/2}^o \rightarrow 2S_{1/2}$	$5.33 \cdot 10^8$	...	1
[Si III]	1882.7	16.34	0.000 - 6.585	$3P_2^o \rightarrow 1S_0$	0.012	$6.4 \cdot 10^4$	1,2,3
Si III]	1892.03	16.34	0.000 - 6.553	$3P_1^o \rightarrow 1S_0$	16700	$2.1 \cdot 10^{11}$	1,4,5
[C III]	1906.7	24.38	0.000 - 6.502	$3P_2^o \rightarrow 1S_0$	0.0052	$7.7 \cdot 10^4$	1,2,6
C III]	1908.734	24.38	0.000 - 6.495	$3P_1^o \rightarrow 1S_0$	114	$1.4 \cdot 10^{10}$	1,2,4,5
Fe III	1914.066	16.18	3.727 - 10.200	$z^7P_3^o \rightarrow a^7S_3$	$6.6 \cdot 10^8$	...	7

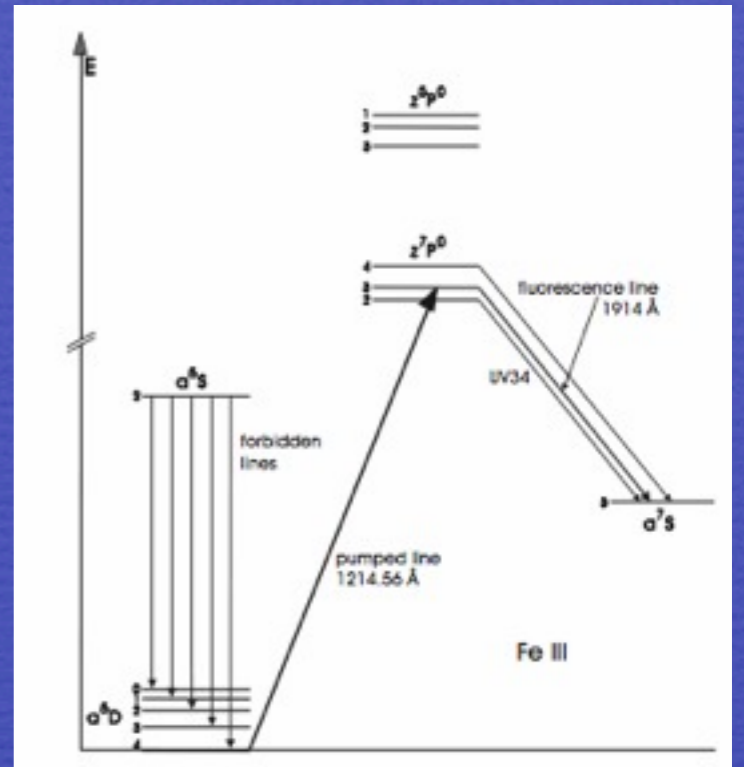
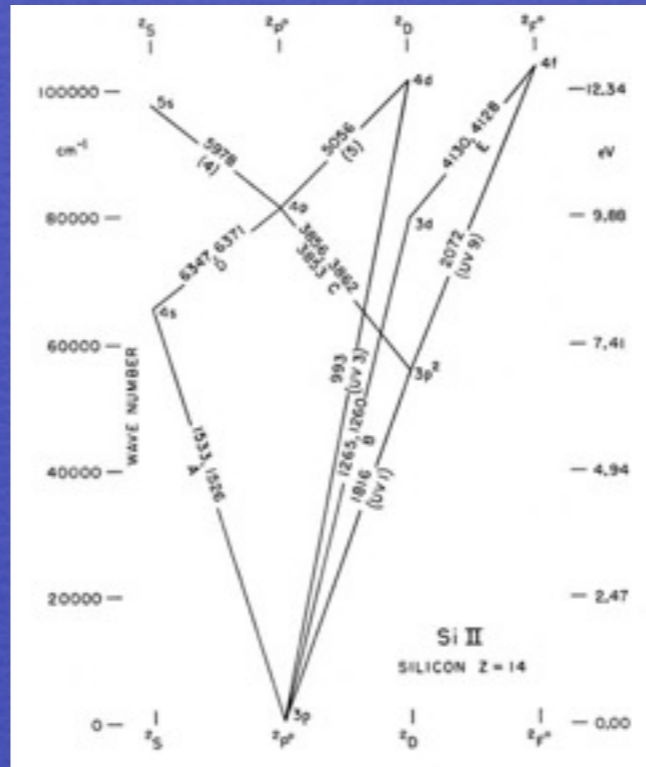
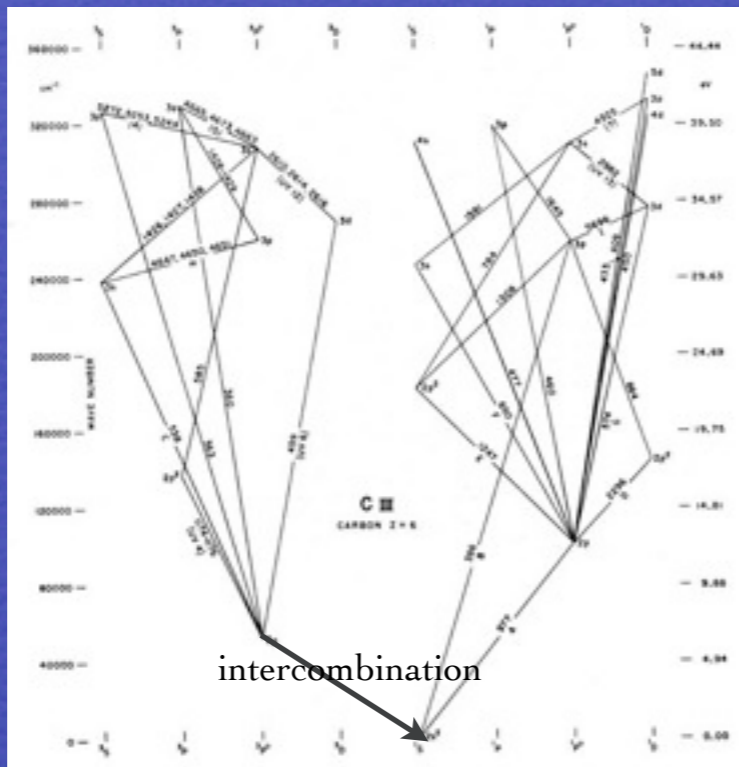
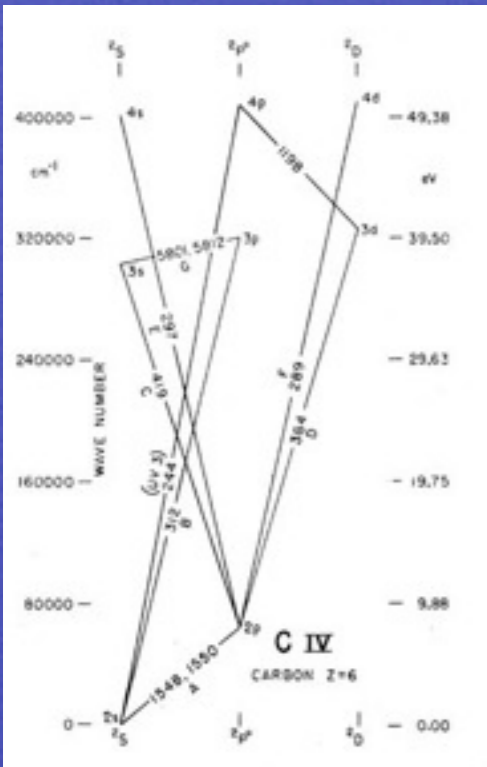
NOTE. — All wavelengths are in vacuum. (1) Ralchenko, Yu., Kramida, A.E., Reader, J., and NIST ASD Team (2008). NIST Atomic Spectra Database (version 3.1.5). Available at: <http://physics.nist.gov/asd3>. 2: Feibelman & Aller (1987). 3:  $n_c$  computed following Shaw & Dufour (1995). 4: Morton (1991). 5: Feldman (1992). 6: Zheng (1988). 7: Wavelength and  $A_{ki}$  from Ekberg (1993), energy levels from Edlén and Swings (1942).

C IV (Al III, Si IV)

C III] (Si III])

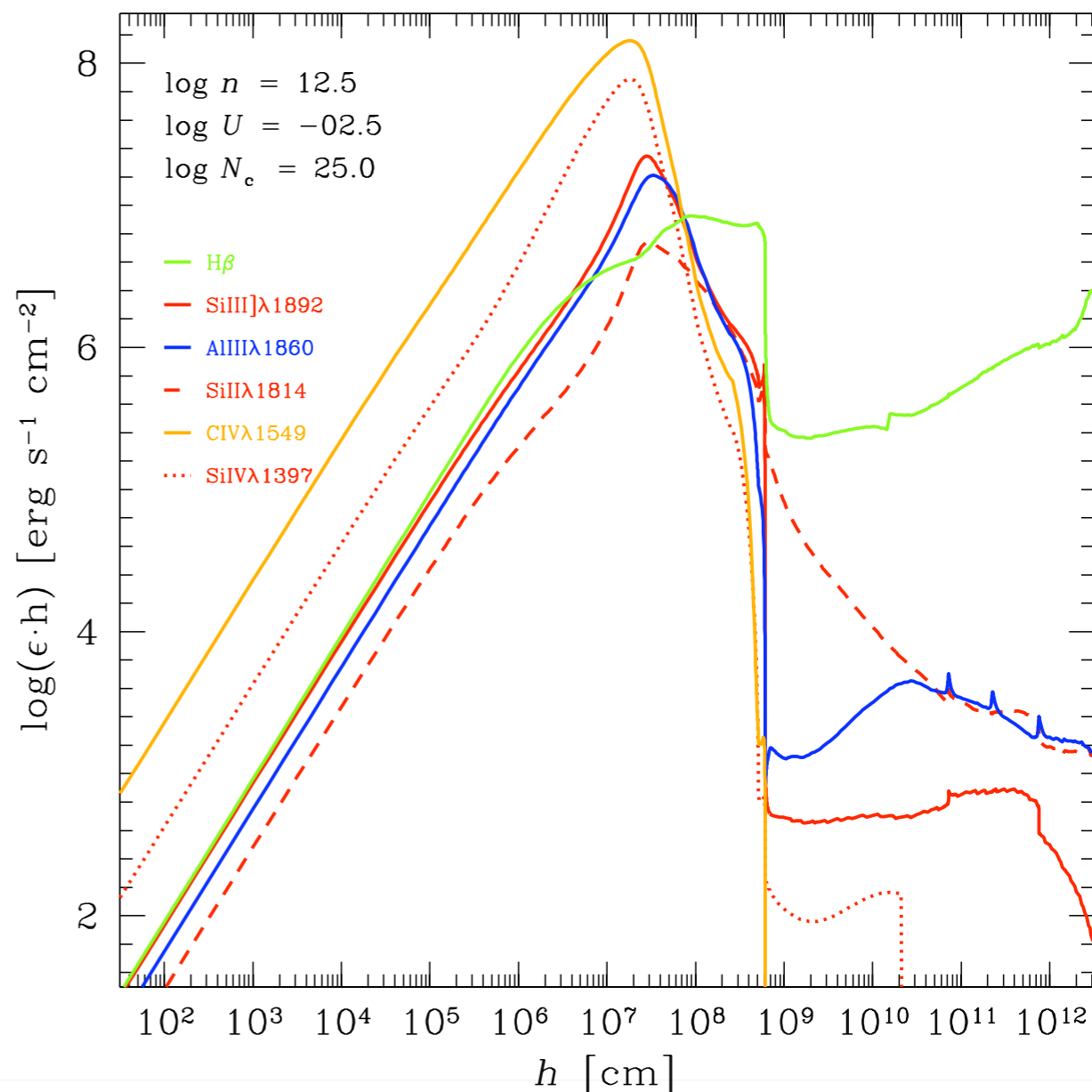
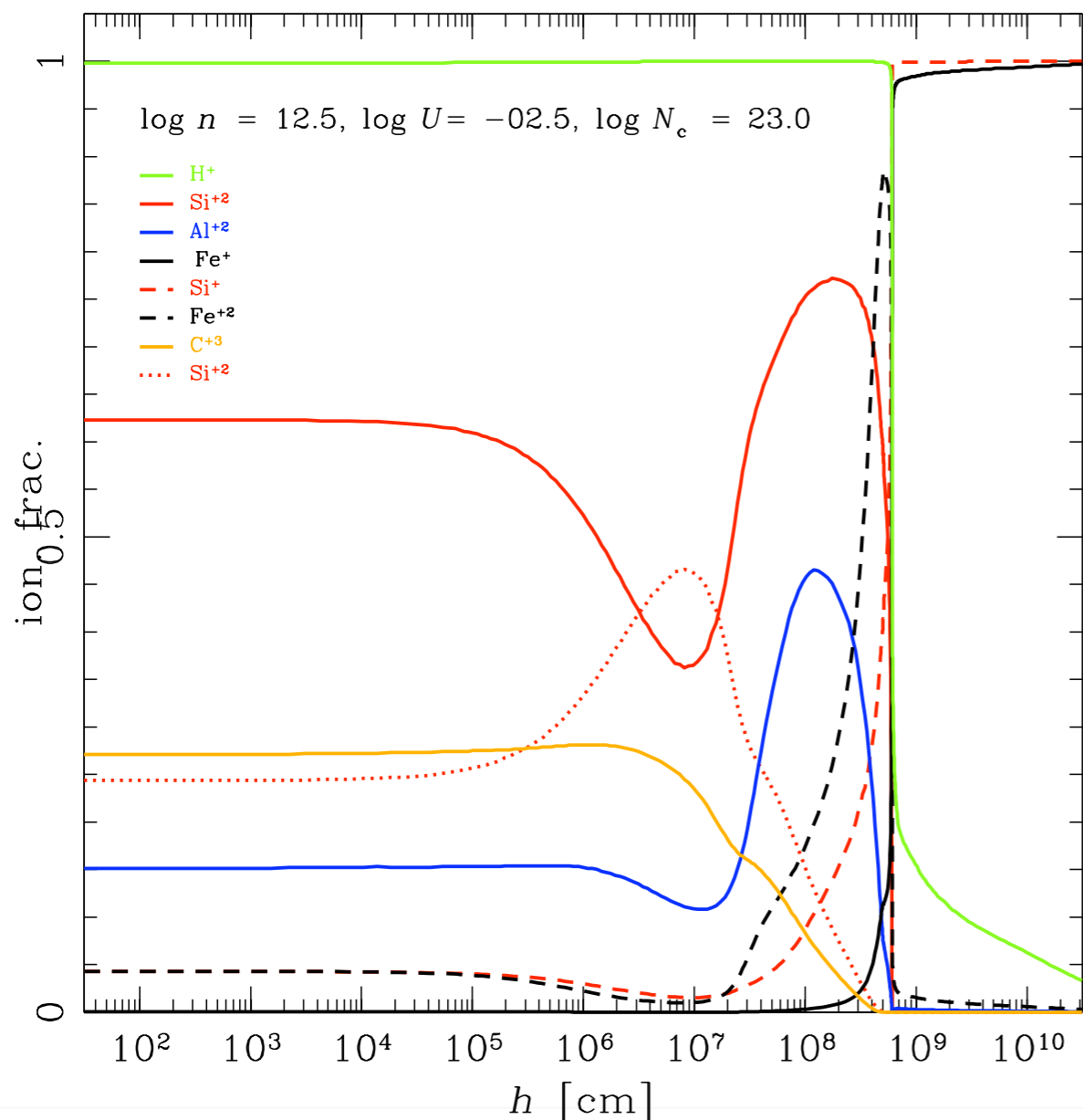
Si II

Fe III  $\lambda$  1914, Ly $\alpha$  pumping



# Ionization structure of the emitting gas slab

# Line emissivity as a function of depth within the slab





# Diagnostic Intensity Ratios

Si IV  $\lambda$ 1397/Si III]  $\lambda$ 1892

Si II 1814/Si III]  $\lambda$ 1892

*independent on metallicity*  
*sensitive to ionization*

C IV  $\lambda$ 1549/Si IV]  $\lambda$ 1397

*sensitive to metallicity*

Al III  $\lambda$ 1860/Si III]  $\lambda$ 1892

*sensitive to density*

C IV  $\lambda$ 1549/Al III  $\lambda$ 1860

*sensitive to ionization*

C IV  $\lambda$ 1549/Si III]  $\lambda$ 1892

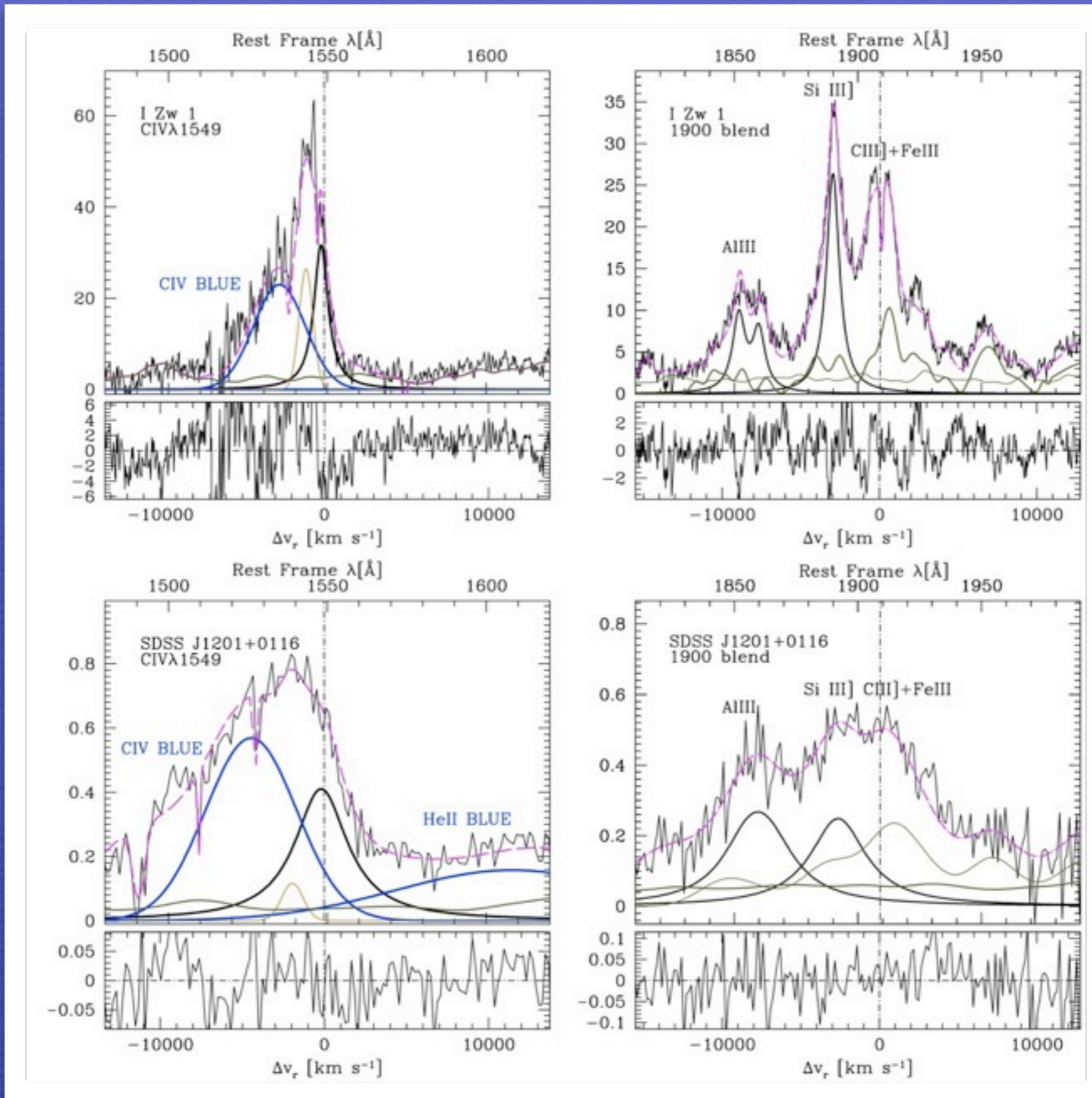
*dependent on metallicity*

Measured with IRAF SPECFIT

along with continuum

Fe II, Fe III emission

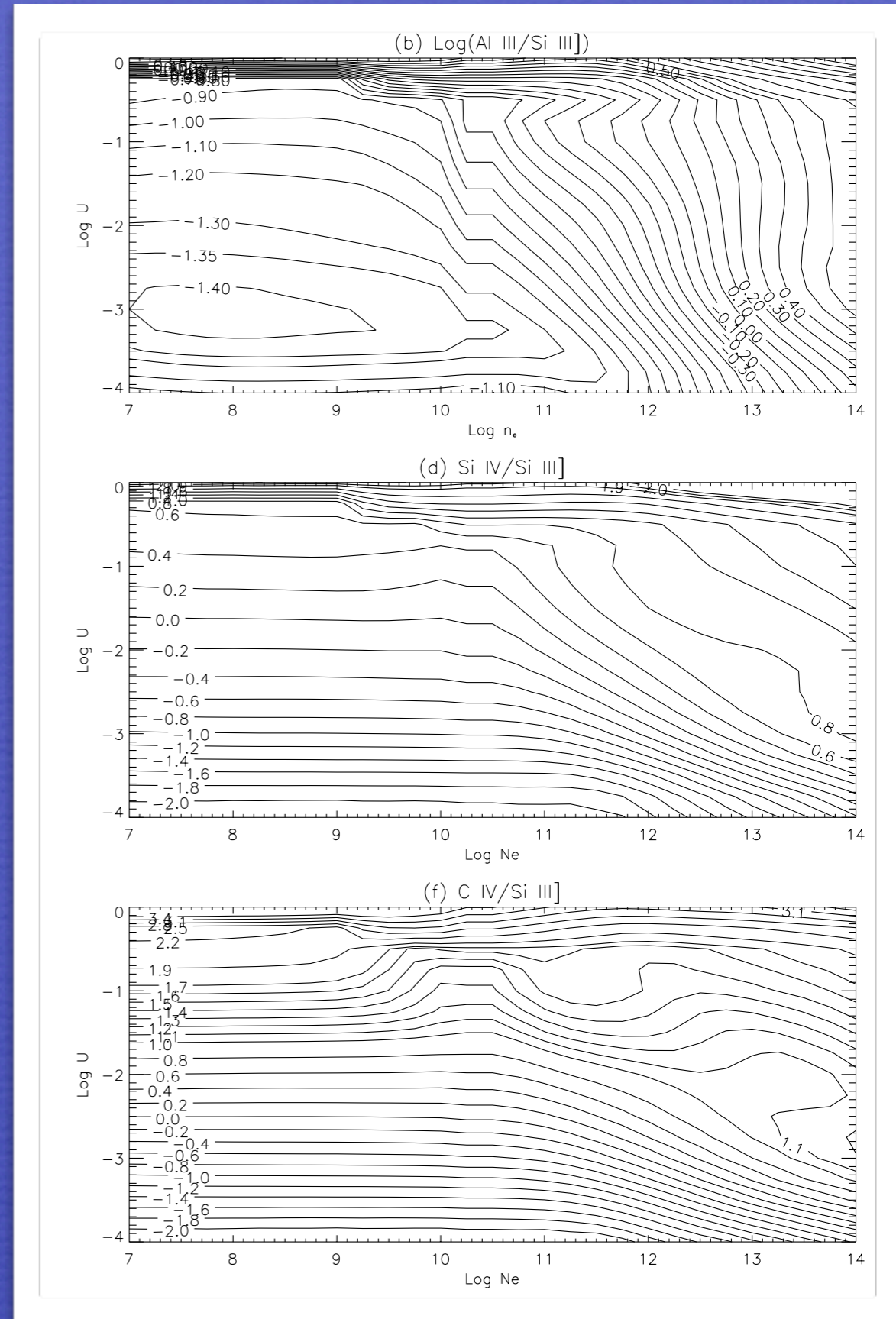
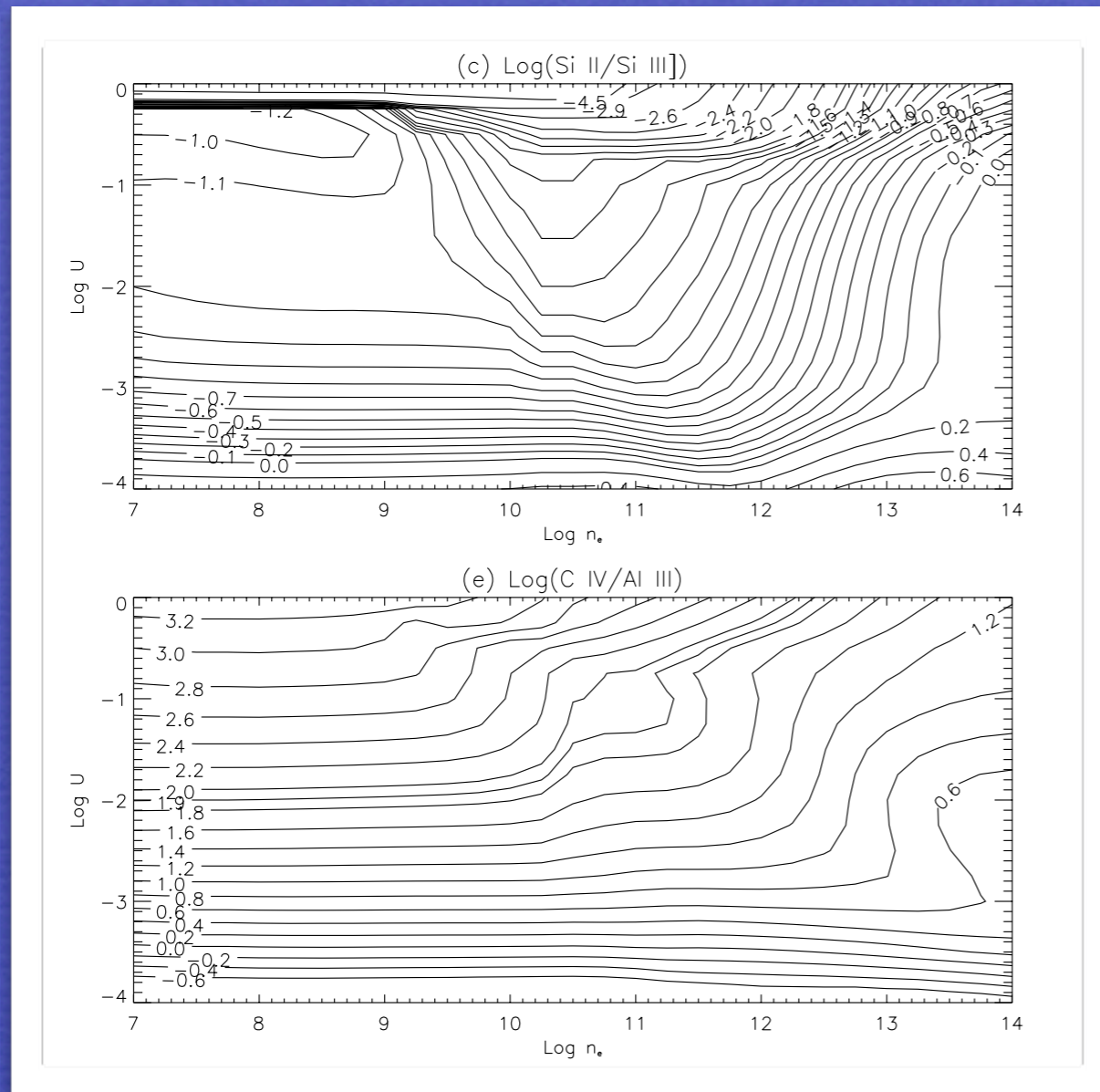
# The targets: high luminosity equivalents of NLSy1s



# CLOUDY 08.00 photoionization computations

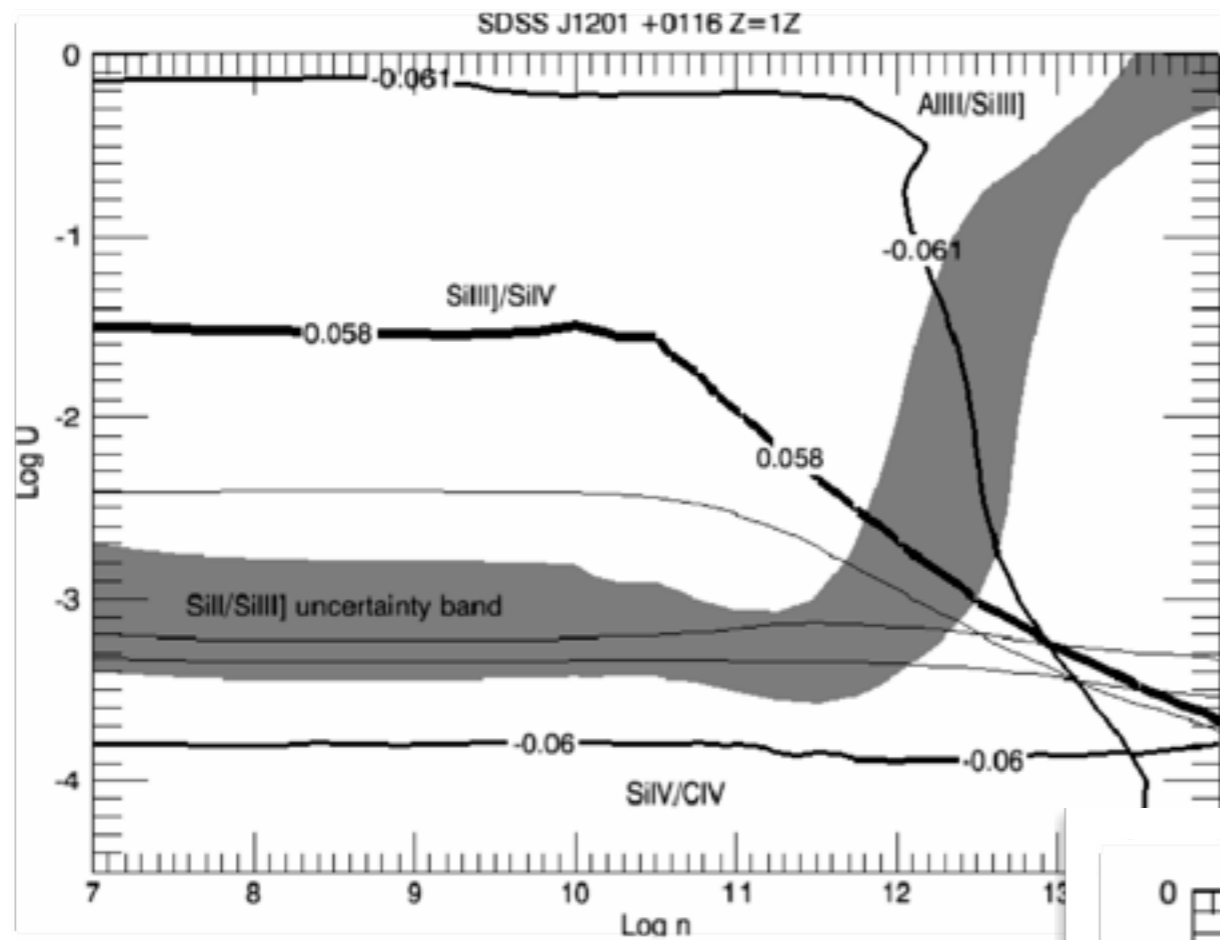
Ferland et al. 1998; cf Korista et al. 1997

19x29 array in logU x logn  
metallicity solar, 5  $Z_{\odot}$ , 5  $Z_{\odot}$  Si-Al enriched  
Ferland & Mathews and Laor et. al. continua  
Column density  $10^{23}$  and  $10^{25}$  cm $^{-2}$

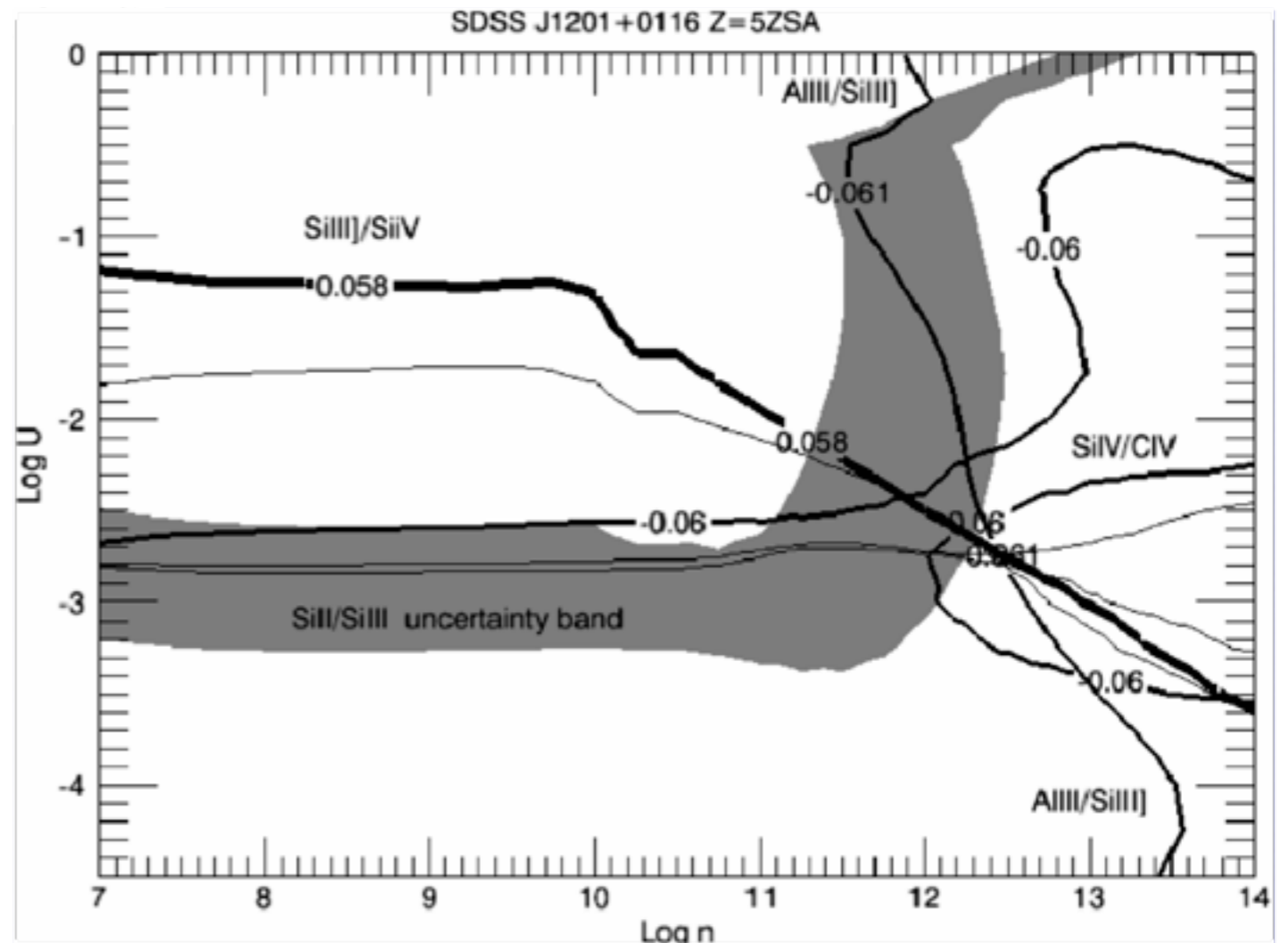


# SDSS J1201+0116

assumption of solar metallicity:  
unsatisfactory, unphysical



5 times solar  
metallicity  
with 3 times Si  
and Al  
enrichment:  
good  
convergence



# Sources of error

diagnostics: less than  $\pm 0.2$  in log

$$r_{\text{BLR}} = \underbrace{\frac{1}{(4\pi c)^{\frac{1}{2}}}}_{\text{const.}} \underbrace{(U n_e)^{-\frac{1}{2}}}_{\text{diagnostics}} \left( \underbrace{\int_{\nu_0}^{+\infty} \frac{L_\nu}{h\nu} d\nu}_{\# \text{ ionizing photons}} \right)^{\frac{1}{2}}$$

$\Delta \log Q(\text{H}) \pm 0.065$  [shape]

$\Delta \log f_\lambda: \pm 0.08$

$\Delta \log r_{\text{BLR}} \approx 0.23$

$$M_{\text{BH}} = \frac{f r_{\text{BLR}} (\text{FWHM})^2}{G}$$

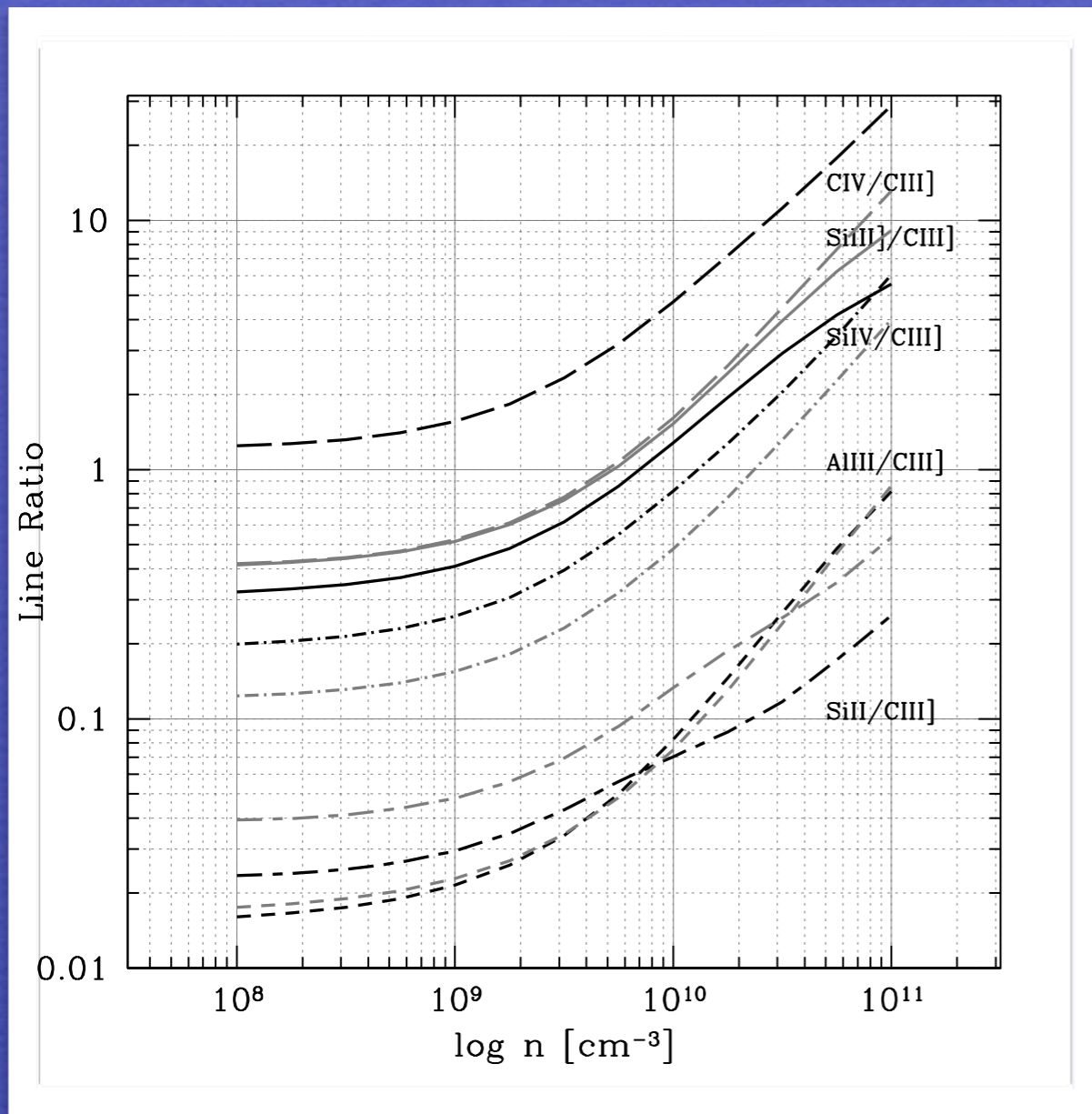
$\Delta \log f \approx$  not set

$\Delta \log \text{FWHM}: \pm 0.16$

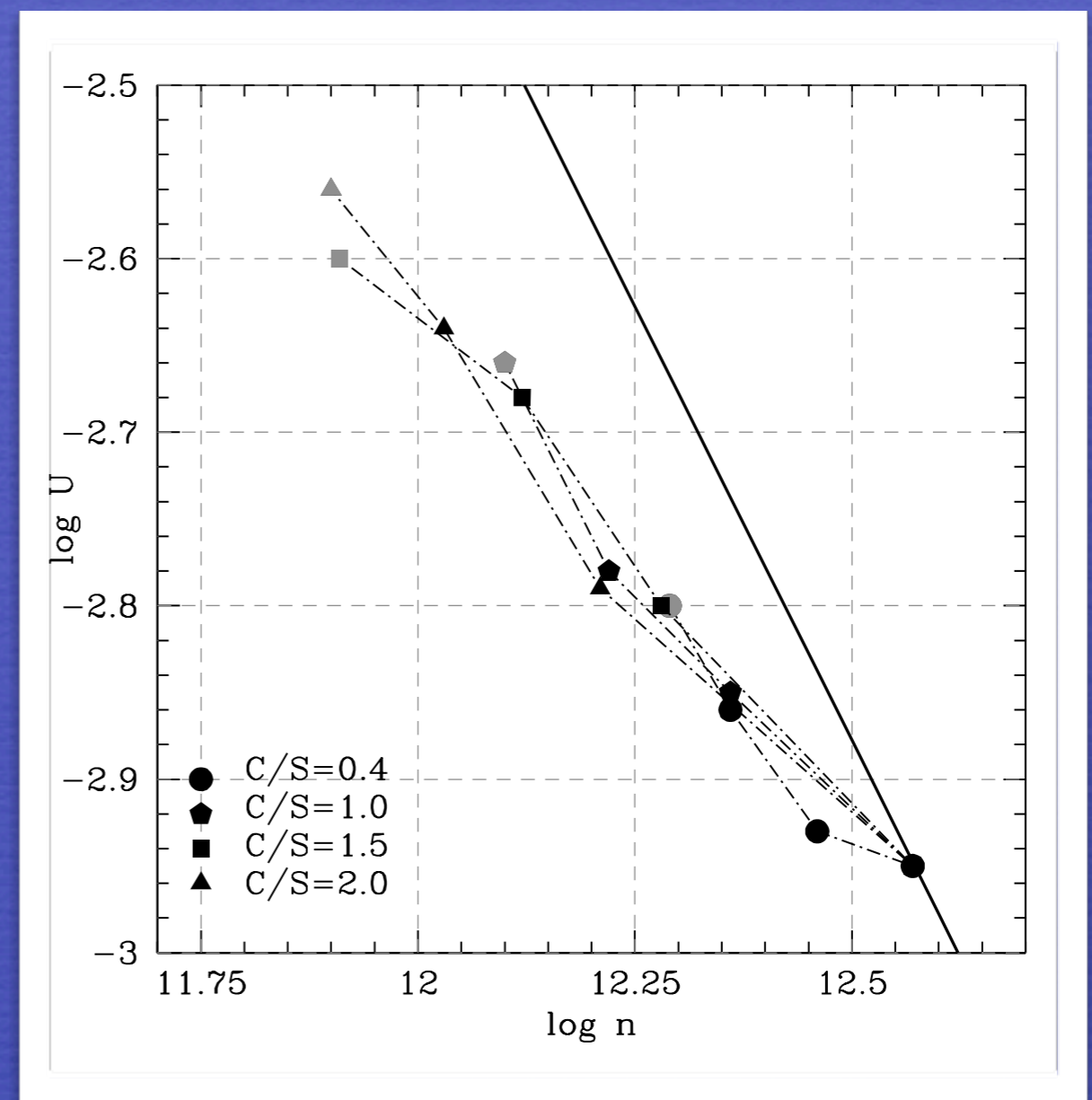
$\Delta \log M_{\text{BH}} \approx 0.3$  ( $2\sigma$  confidence)

# Can the method be applied to the general population of quasars?

CIII] and VBC (Pop. B) complicate the issue but do not make it hopeless

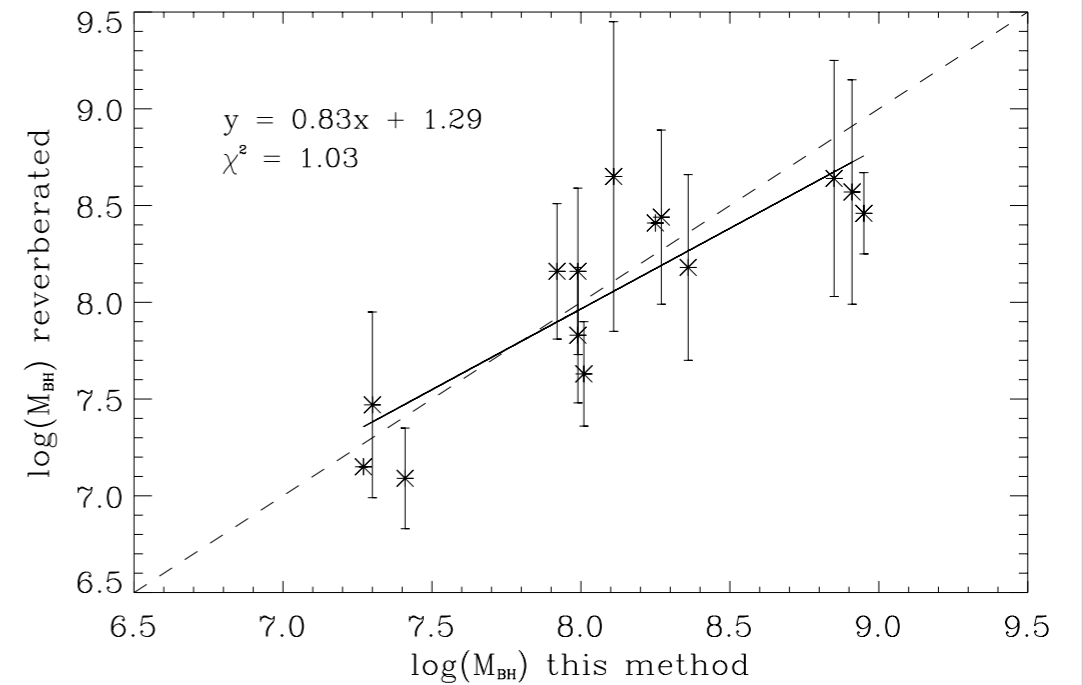
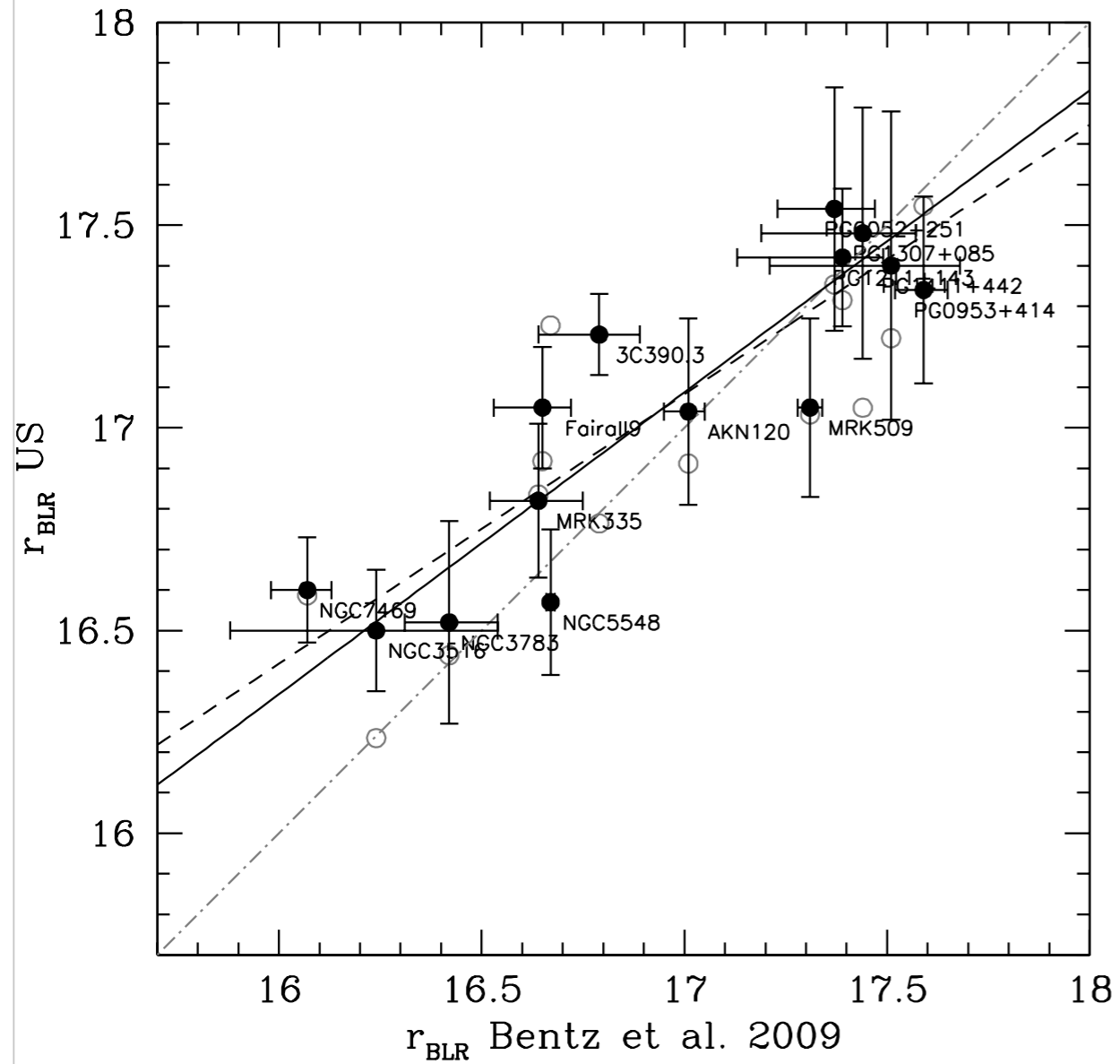


$\log \Gamma = -2; \log \Gamma = -5$



assumes  $\log \Gamma = -2$

# Reverberation-mapped objects



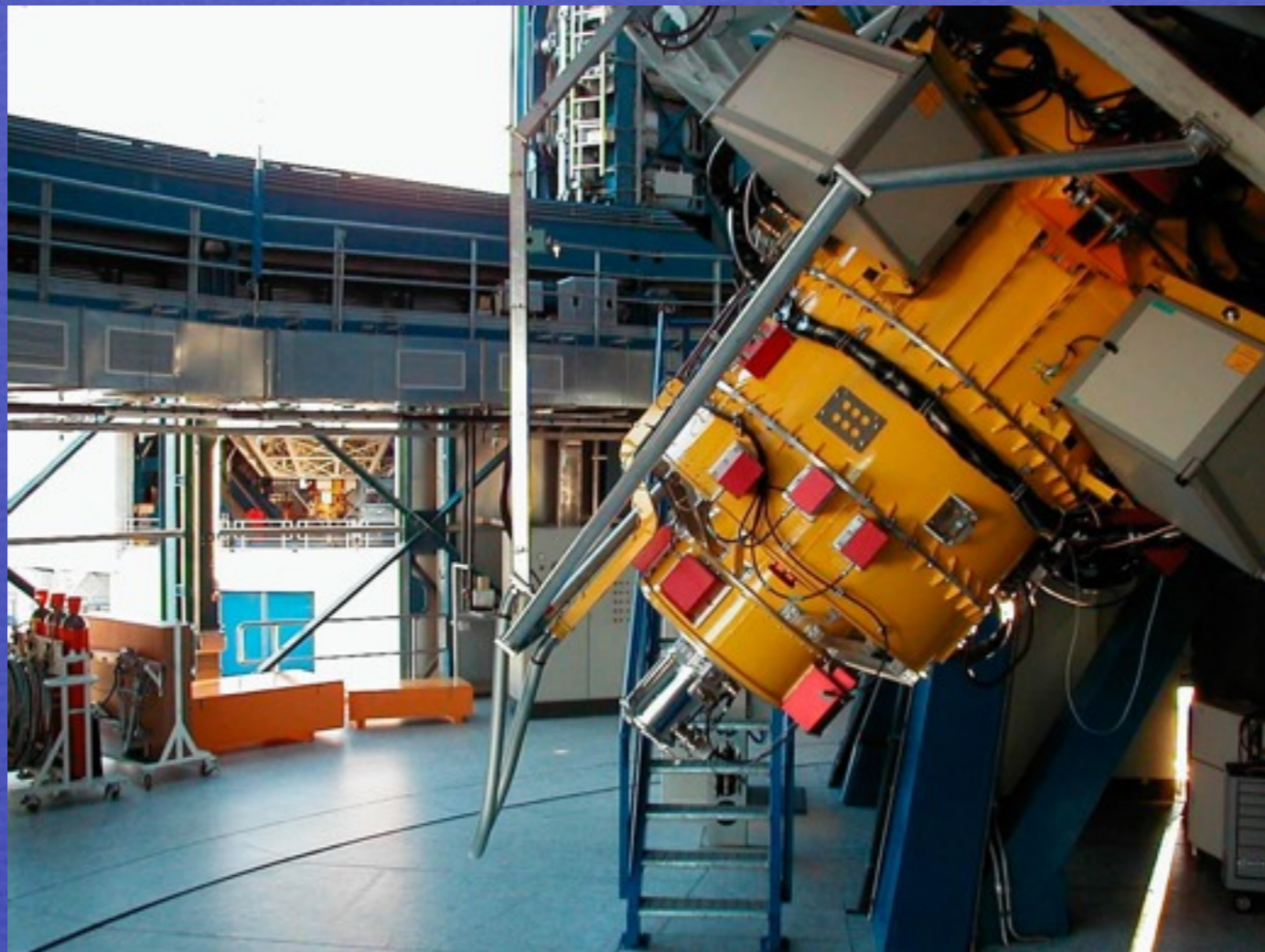
Negrete et al., in preparation

# Toward higher redshift ...

ESO  
VLT

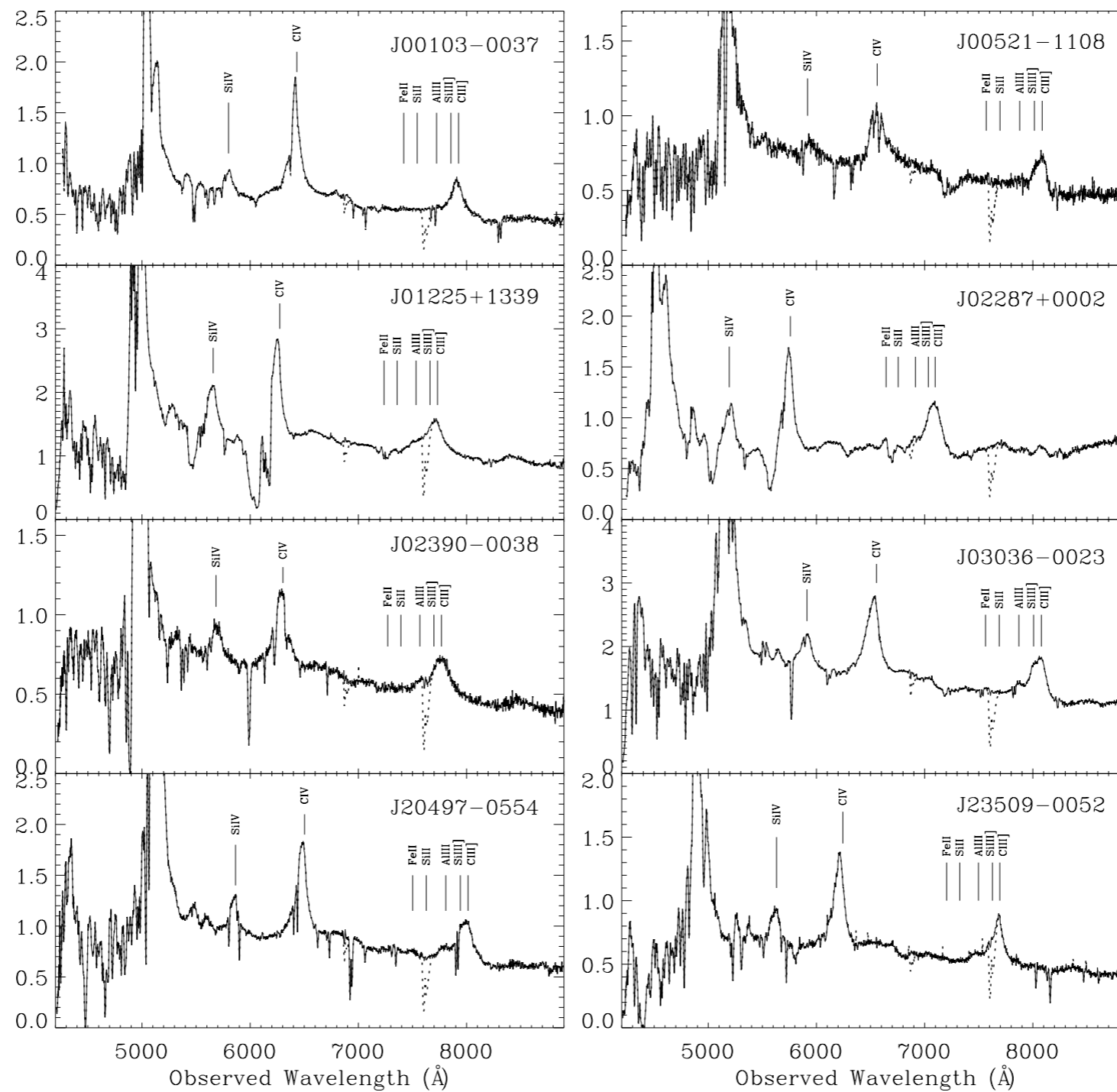


FORS

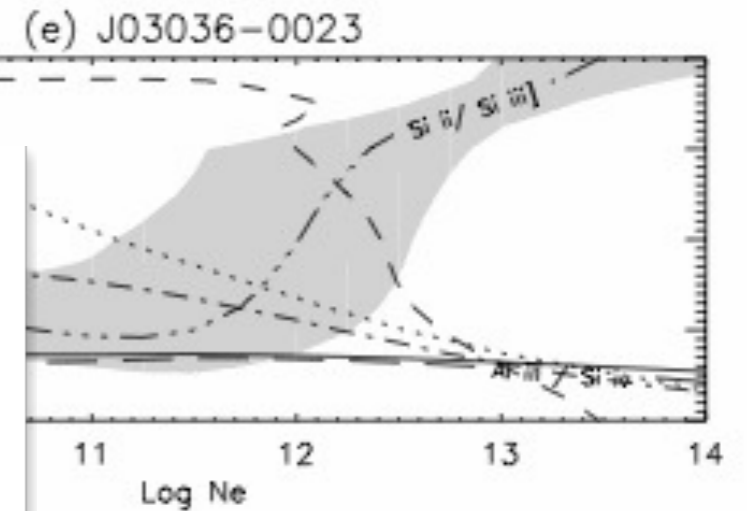
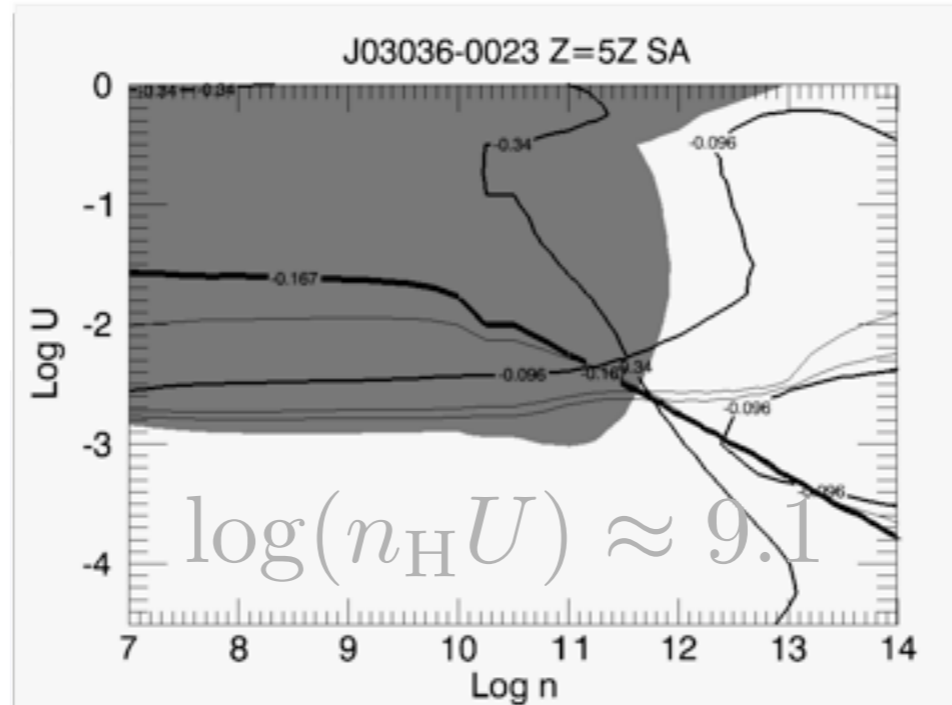
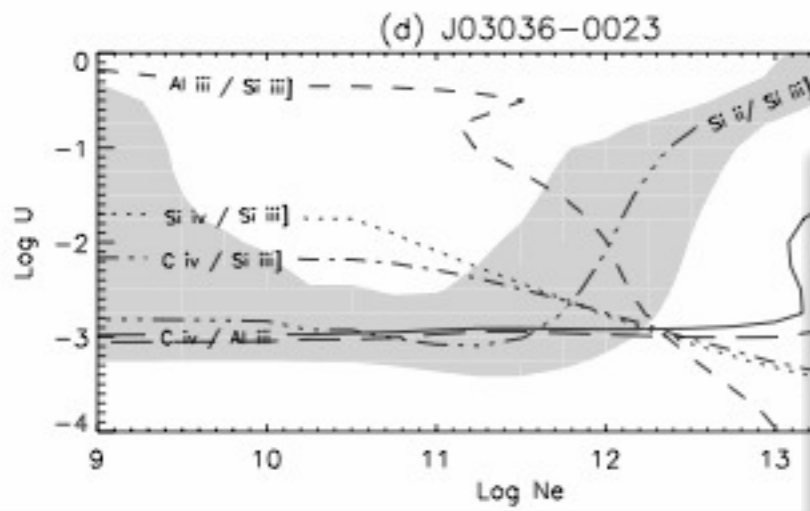
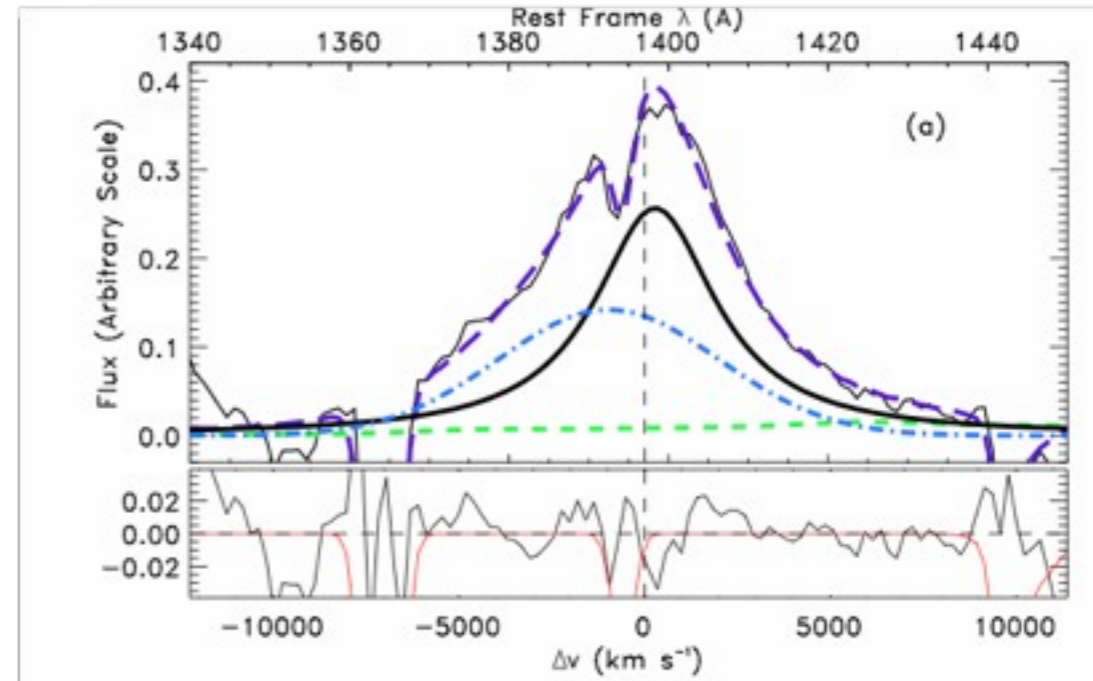
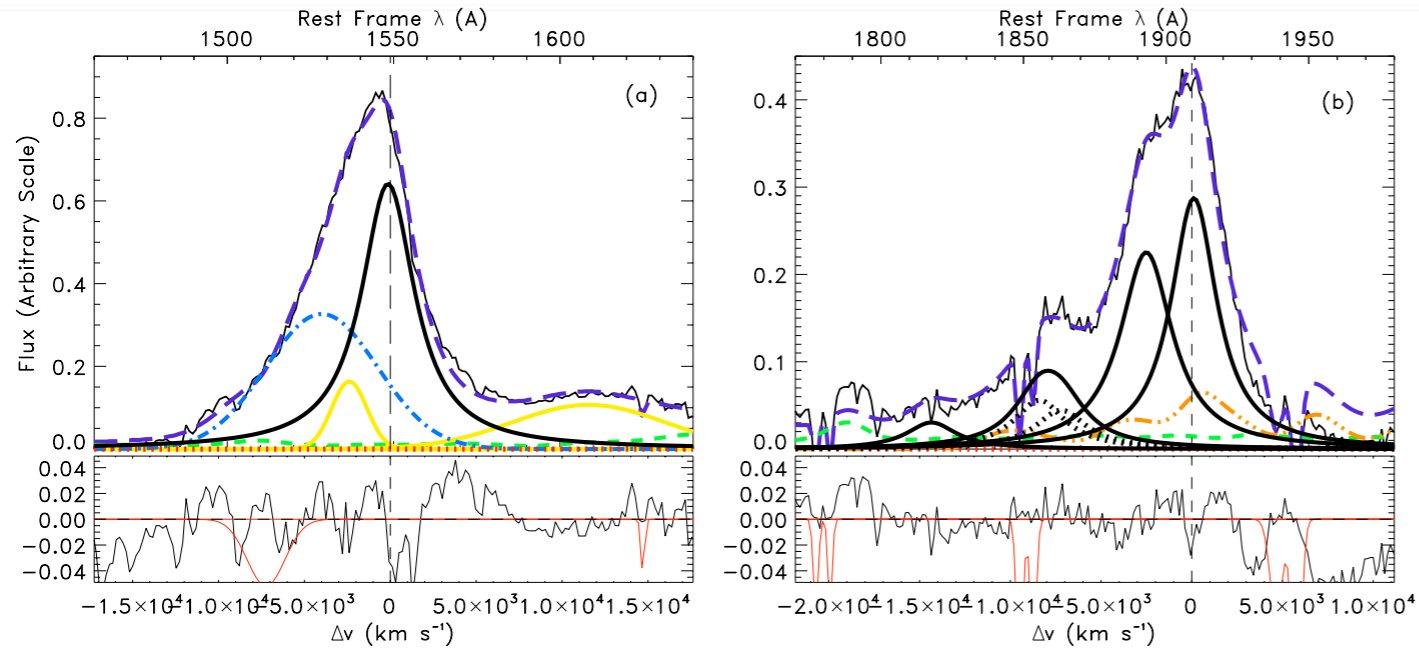




# Pilot observations with FORS



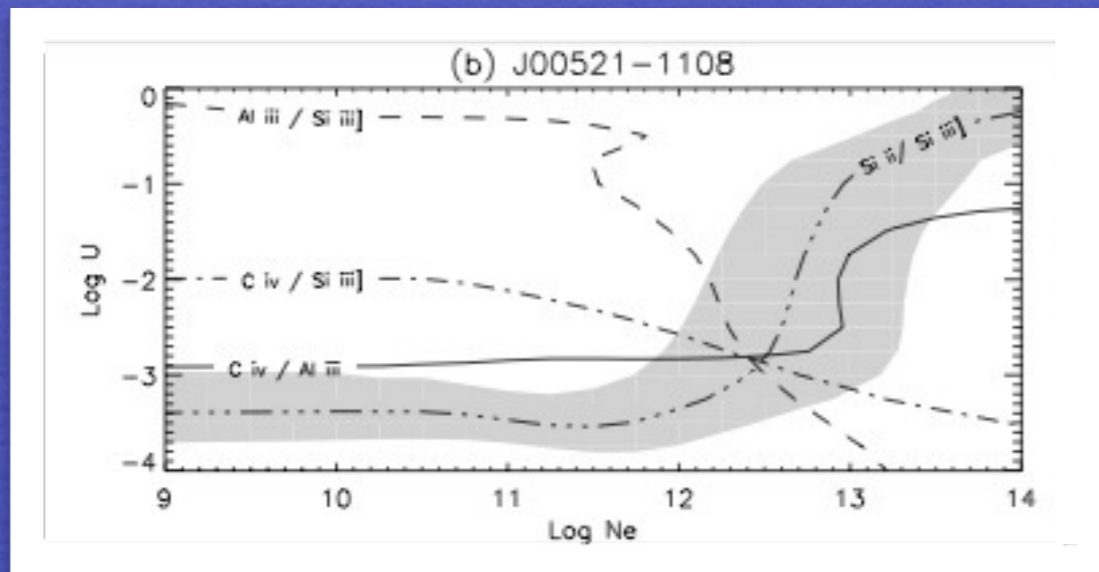
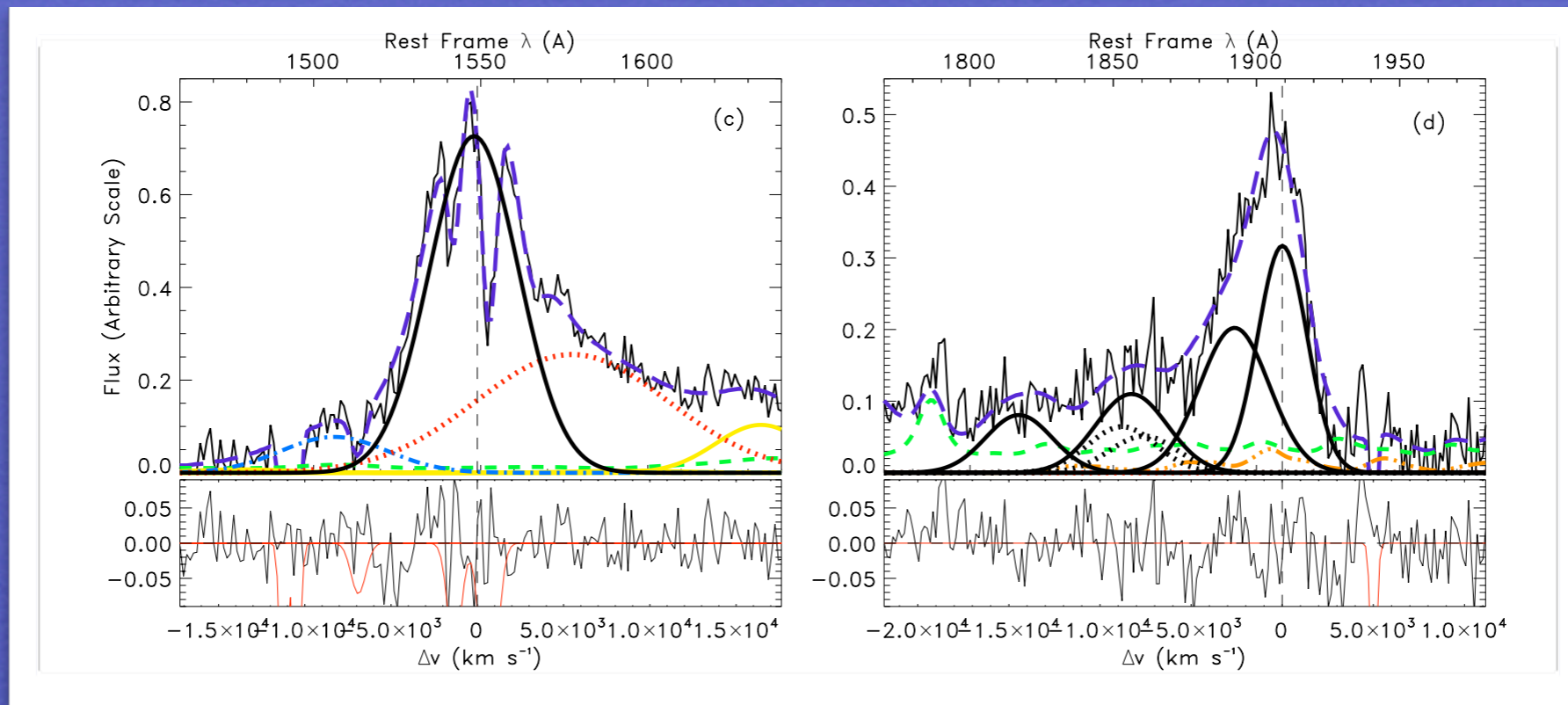
# J03036-0023



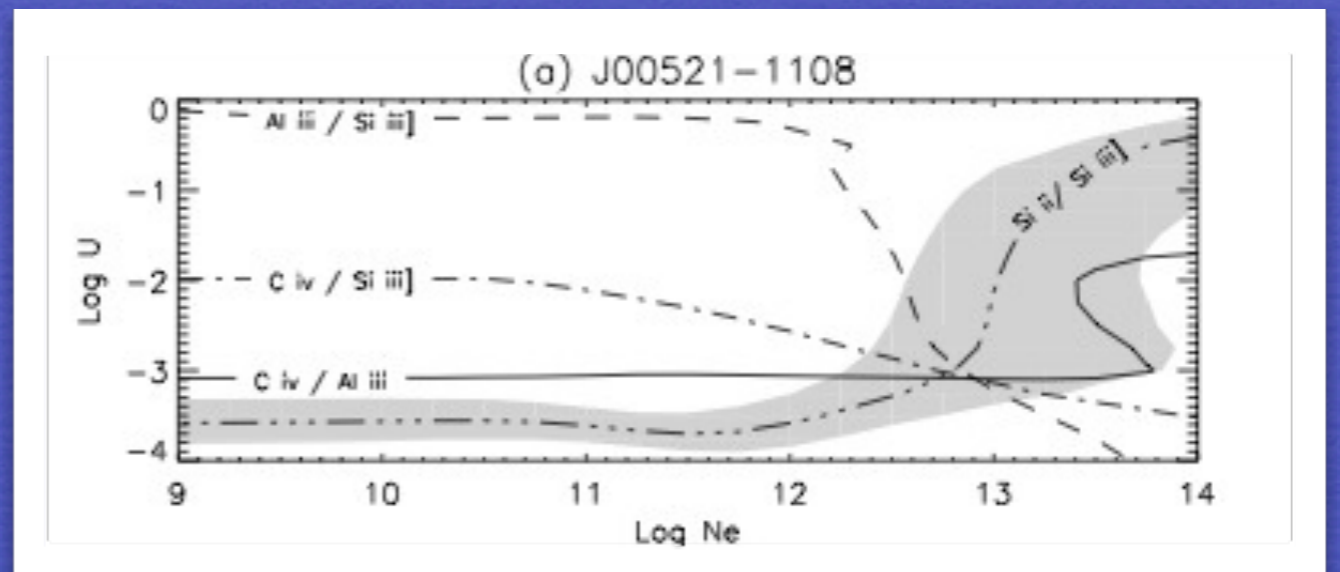
$$\log(n_{\text{H}}U) \approx 9.4$$

$$\log(n_{\text{H}}U) \approx 9.1$$

# J00521-1108

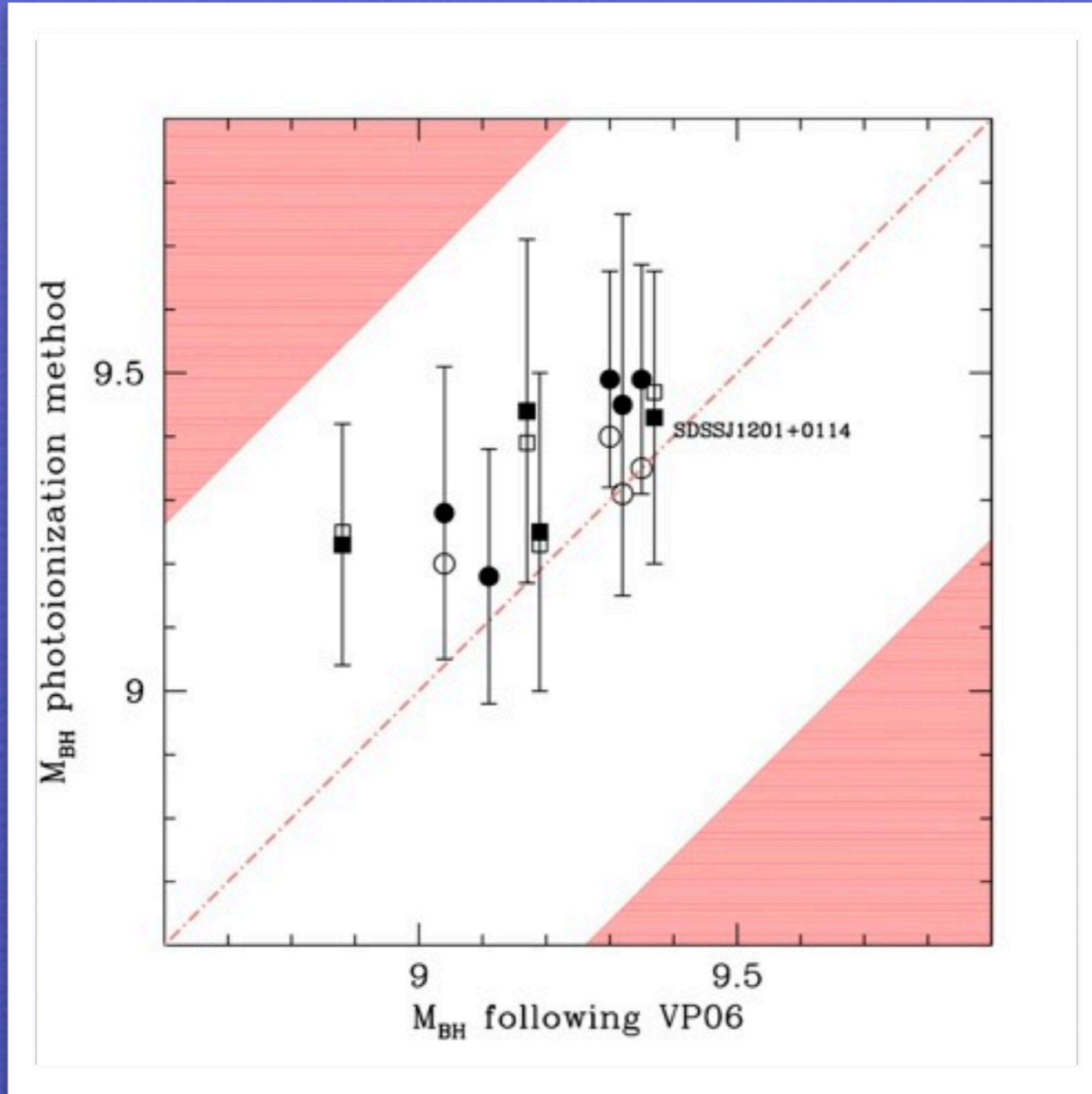


$$\log(n_{\text{H}}U) \approx 9.6$$



$$\log(n_{\text{H}}U) \approx 9.85$$

# $M_{\text{BH}}$ for high- $z$ quasars with FORS spectra



Comparison with  
 $M_{\text{BH}}$  from  
 CIV  $L$  correlation

NB: both measures  
 $\propto L^{1/2}$

Negrete et al. 2011, submitted

$$\log M_{\text{BH}}(\text{CIV}) = \log \left\{ \left[ \frac{\text{FWHM}(\text{CIV})}{1000 \text{ km s}^{-1}} \right]^2 \left[ \frac{\lambda L_{\lambda}(1350\text{\AA})}{10^{44} \text{ ergs s}^{-1}} \right]^{0.53} \right\} + (6.66 \pm 0.01) - s_f$$

Vestergaard & Peterson 2006

# Sources of concern

fundamental assumptions  
photoionization, spherical symmetry  
one density, one ionization parameter:  
clearly an oversimplification

predicted line intensities  
lack of perfect convergence

measurements of line fluxes (S/N, dispersion, deblending)  
coarse assumptions on metallicity  
continuum shape, anisotropy  
all errors in the conventional application  
of the virial mass relationship

# Conclusions

The described photoionization method:

works best for NLSy1-like sources at high redshift

with ideal dataset allows determination of  
density, ionization, and metallicity

works for other sources as far as the  $(nU)$  is sought  
but reliability difficult to assess

probably lower uncertainty  
than method based on the  $L-r_{\text{BLR}}$  correlation

requires high S/N and moderate dispersion  
but can in principle be applied to very high  $z$  ( $>6.5$ )

# Downsizing?

